10
Heavy quarks

One of the motivations for collider experiments is to discover new heavy objects. It is therefore important to test our understanding of such processes by predicting the production rates for the known heavy objects, such as the top, bottom and charm quarks, and to compare the predictions with experimental measurements.

Aspects of the production of heavy quarks in e^+e^- annihilation have already been considered in Chapter 3. We shall concentrate here on the hadronic production of heavy quarks. An idea of the relative cross sections and signal-to-background ratios for c, b and t quark production at various present and future accelerators can be obtained from Table 10.1. As we shall see, the description of hadronic production is possible in perturbative QCD when the mass of the produced quark is large compared to 1 GeV, the typical scale of the strong interactions. Because the cross sections are generally large, hadronic interactions offer the potential to produce the large number of heavy quarks necessary to study their decays in detail. However, at present, much of the information on states containing c and b quarks comes from e^+e^- annihilation, because of the better signal-to-background ratios at e^+e^- colliders.

As an illustration of the power of hadron colliders we consider the case of b production. For example, at the Fermilab Tevatron running at a luminosity of 2×10^{31} cm^{-2}s^{-1}, b quarks are produced at 400 Hz. This should be contrasted with an e^+e^- machine such as CESR operating at a luminosity of 2×10^{32} cm^{-2}s^{-1}, where the rate of b production is ~ 0.1 Hz[1]. A large sample of bs is necessary to observe CP violation in the decays of

[1] A large effort is put into upgrading the luminosities of colliding beam machines. These numbers will soon be out of date.

Downloaded from https://www.cambridge.org/core. UNIVERSIDAD AUTONOMA METROPOLITANA, on 17 Nov 2026 at 02:28:30, subject to the Cambridge Core terms of use, available at https://www.cambridge.org/core/terms. https://doi.org/10.1017/CBO9780511628788.011

Process	$\sqrt{s}$ [GeV]	Cross section	$\sigma_{Q\bar{Q}}/\sigma_{tot}$
$\pi N \to c\bar{c}$	25	20 μb	0.1%
$pN \to c\bar{c}$	38	40 μb	0.1%
$\gamma N \to c\bar{c}$	19	0.7 μb	0.4%
$pp \to b\bar{b}$	40	20 nb	10^{-6}
$p\bar{p} \to b\bar{b}$	1800	20 μb	0.03%
$pp \to b\bar{b}$	14000	300 μb	0.5%
$e^+e^- \to b\bar{b}$	10.48	1 nb	25%
$e^+e^- \to b\bar{b}$	91	7 nb	15%
$p\bar{p} \to t\bar{t}$	1800	5 pb	10^{-10}
$pp \to t\bar{t}$	14000	800 pb	10^{-8}
$e^+e^- \to t\bar{t}$	500	500 fb	5%

Table 10.1. Approximate rates for heavy quark production.

hadrons containing b quarks and to measure $B_s - \overline{B}_s$ mixing. In addition, hadronic production of b quarks gives access to a wide spectrum of states, including mesons containing both bottom and charm ($b\bar{c}$) and baryonic states containing b quarks. This is in contrast to e^+e^- machines operating at the $\Upsilon(4S)$ resonance where only the lowest-lying B^0 and B^+ states are produced.

The disadvantage of hadronically produced heavy quarks is that they have to be distinguished from a large background of other hadrons. Table 10.1 shows the discrimination against background which is necessary. This is achieved by using the special properties of the decay products to trigger on the interesting events.

10.1 Charm and bottom quark decays

The existence of hadrons containing heavy quarks is deduced by observation of their decays. Therefore any experiment which measures the cross section for the production of hadrons containing heavy quarks must make assumptions concerning the branching fraction to the observed mode. Since leptons play an important role in the identification of heavy quarks we will begin by discussing semi-leptonic decays.

Downloaded from https://www.cambridge.org/core. UNIVERSIDAD AUTONOMA METROPOLITANA, on 17 Nov 2026 at 02:28:30, subject to the Cambridge Core terms of use, available at https://www.cambridge.org/core/terms. https://doi.org/10.1017/CBO9780511628788.011

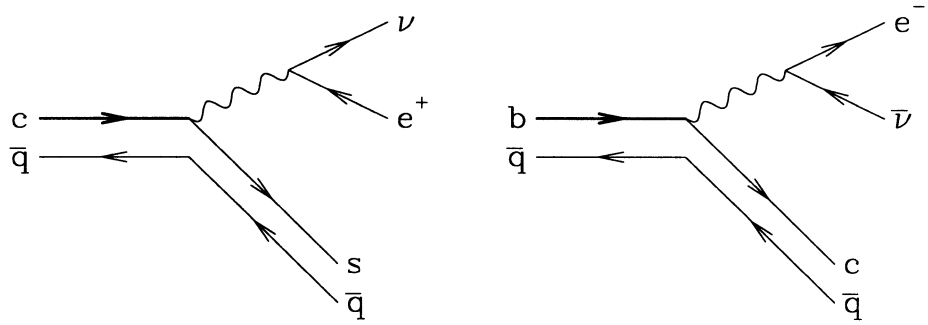


Fig. 10.1. CKM-favoured spectator diagrams for c and b meson decay.

10.1.1 Semi-leptonic decays

The simplest approach is to treat the semi-leptonic decays of hadrons containing c and b quarks in analogy with the decay of a free muon. This is called the *spectator model*, since the quarks which accompany the heavy quark Q in the hadron are assumed to play no role in the decay.

The Lagrangian responsible for the semi-leptonic decay of a c or b quark has the normal $V-A$ structure familiar from muon decay, apart from the factor V_{qQ} coming from the Cabibbo-Kobayashi-Maskawa (CKM) matrix defined in Section 8.3.3. For the moment we consider only the CKM-favoured decays, for which the Lagrangians are

$$\mathcal{L}^{(c)} = -\frac{G_F}{\sqrt{2}} V_{cs}\, \bar{s}\gamma^\mu(1-\gamma_5)c\, \bar{\nu}\gamma_\mu(1-\gamma_5)e\,, \tag{10.1}$$

$$\mathcal{L}^{(b)} = -\frac{G_F}{\sqrt{2}} V_{cb}\, \bar{c}\gamma^\mu(1-\gamma_5)b\, \bar{e}\gamma_\mu(1-\gamma_5)\nu\,. \tag{10.2}$$

The generalization to CKM-disfavoured decays is straightforward. The diagrams responsible for these decays are shown in Fig. 10.1. The matrix elements for c and b decay, taking into account the finite masses of the quarks, are

$$\begin{aligned} \overline{\sum}|\mathcal{M}^{(c)}|^2 &= 64 G_F^2\, |V_{cs}|^2\, c\cdot e^+\, s\cdot\nu\,, \\ \overline{\sum}|\mathcal{M}^{(b)}|^2 &= 64 G_F^2\, |V_{cb}|^2\, b\cdot\bar{\nu}\, c\cdot e^-\,, \end{aligned} \tag{10.3}$$

where $b, c, s, \nu, \bar{\nu}, e^+$ and e^- now stand for the four-momenta of the particles in the decay. The structure of the matrix elements given in Eq. (10.3) has already been commented on in our discussion of the angular distribution in W decay in Chapter 9. In the standard model, the $V-A$ form of the charged weak current determines that fermions participating in weak decay are predominantly left-handed and antifermions predominantly right-handed. Consequently angular momentum conservation dic-

Downloaded from https://www.cambridge.org/core. UNIVERSIDAD AUTONOMA METROPOLITANA, on 17 Nov 2026 at 02:28:30, subject to the Cambridge Core terms of use, available at https://www.cambridge.org/core/terms. https://doi.org/10.1017/CBO9780511628788.011

tates that the s and ν momenta prefer to be anti-parallel in c quark decay. The endpoint configuration in which the e^+ recoils against the parallel s and ν is thus disfavoured. We therefore expect a soft spectrum for the positron coming from the decay of a charm meson. Conversely we expect a hard spectrum for the neutrino (or for the electron coming from the decay of a b quark). These features are apparent in the matrix elements, Eq. (10.3).

The semi-leptonic decay rate is obtained by including the three-particle phase space and flux factor as follows:

$$\Gamma_{\rm sl}^{(Q)} = \frac{m_Q}{2^8\pi^3}\int dxdy\;\theta(x+y-x_m)\;\theta(x_m-x-y+xy)\;\overline{\sum}|\mathcal{M}^{(Q)}|^2 \quad (10.4)$$

where x and y are the rescaled energies of the charged and neutral leptons, $x = 2E_e/m_Q$, $y = 2E_\nu/m_Q$ in the frame in which the heavy quark Q is at rest. The kinematic endpoint of the spectrum is denoted by x_m and is given by $x_m = 1-\epsilon^2$ where $\epsilon = m_q/m_Q$. The parameter ϵ is equal to m_s/m_c for c decay and equal to m_c/m_b for b decay. The result for the semi-leptonic widths of the c and the b is

$$\begin{aligned}\frac{d\Gamma_{\rm sl}^{(c)}}{dxdy} &= |V_{cs}|^2\Gamma_0(m_c)[12x(x_m-x)]\\ \frac{d\Gamma_{\rm sl}^{(b)}}{dxdy} &= |V_{cb}|^2\Gamma_0(m_b)[12y(x_m-y)] \qquad (10.5)\end{aligned}$$

where Γ_0 is the rescaled muon decay rate,

$$\Gamma_0(m_Q) = \frac{G_F^2 m_Q^5}{192\pi^3}\,. \qquad (10.6)$$

The lepton spectra calculated from Eq. (10.5) are

$$\frac{d\Gamma_{\rm sl}^{(c)}}{dx} = |V_{cs}|^2\Gamma_0(m_c)\left[\frac{12x^2(x_m-x)^2}{(1-x)}\right] \qquad (10.7)$$

$$\frac{d\Gamma_{\rm sl}^{(b)}}{dx} = |V_{cb}|^2\Gamma_0(m_b)\left[\frac{2x^2(x_m-x)^2}{(1-x)^3}\right](6-6x+xx_m+2x^2-3x_m). \qquad (10.8)$$

These spectra are plotted in Fig. 10.2. Note that, as expected, the e^+ from charm decay has a soft spectrum. The form of the lepton spectrum from b decay is of great interest. The electron spectrum for the CKM-disfavoured mode $b\to u$ is hard. The measurement of leptons with energies beyond the kinematic limit for $b\to c$ [1] is the primary method by which information about V_{ub} is obtained. The value derived for V_{ub} depends in detail on the form of the lepton spectrum in the endpoint region, which may

Downloaded from https://www.cambridge.org/core. UNIVERSIDAD AUTONOMA METROPOLITANA, on 17 Nov 2026 at 02:28:30, subject to the Cambridge Core terms of use, available at https://www.cambridge.org/core/terms. https://doi.org/10.1017/CBO9780511628788.011

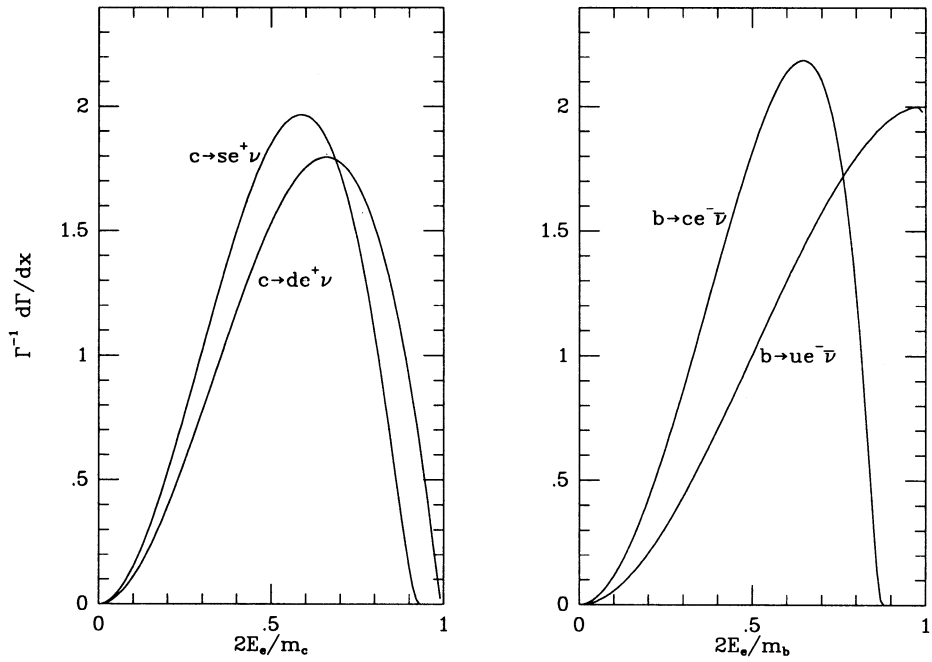


Fig. 10.2. Shapes of the lepton spectra in c and b decay.

not be well predicted by the simple spectator model [2]. Allowing for this theoretical uncertainty, the measured value is $|V_{ub}/V_{cb}| = 0.08 \pm 0.02$ [3].

After integration of either Eq. (10.7) or Eq. (10.8), the semi-leptonic width including mass effects is found to be

$$\Gamma_{\rm sl}^{(Q)} = |V_{Qq}|^2 \Gamma_0(m_Q) f\left(\frac{m_q}{m_Q}\right) \tag{10.9}$$

where the function f is given by

$$f(\epsilon) = (1-\epsilon^4)(1-8\epsilon^2+\epsilon^4) - 24\epsilon^4 \ln \epsilon \,. \tag{10.10}$$

Including the CKM-disfavoured mode $c \to d$ the result for the semi-leptonic decay of the c quark is

$$\Gamma_{\rm sl}^{(c)} = \Gamma_0(m_c)\Big[f(m_s/m_c)|V_{cs}|^2 + f(m_d/m_c)|V_{cd}|^2\Big]. \tag{10.11}$$

This expression has a large numerical uncertainty dependent on the value chosen for the charm quark mass. The result is also subject to strong interaction corrections; since we are interested here in a rough check of the model, we ignore these for the case of charm. If we take a value of $m_c = 1.4$ GeV, the theoretical estimate for the semi-leptonic width is

$$\Gamma_{\rm sl} = 1.1 \times 10^{-10} \text{ MeV}. \tag{10.12}$$

Downloaded from https://www.cambridge.org/core. UNIVERSIDAD AUTONOMA METROPOLITANA, on 17 Nov 2026 at 02:28:30, subject to the Cambridge Core terms of use, available at https://www.cambridge.org/core/terms. https://doi.org/10.1017/CBO9780511628788.011

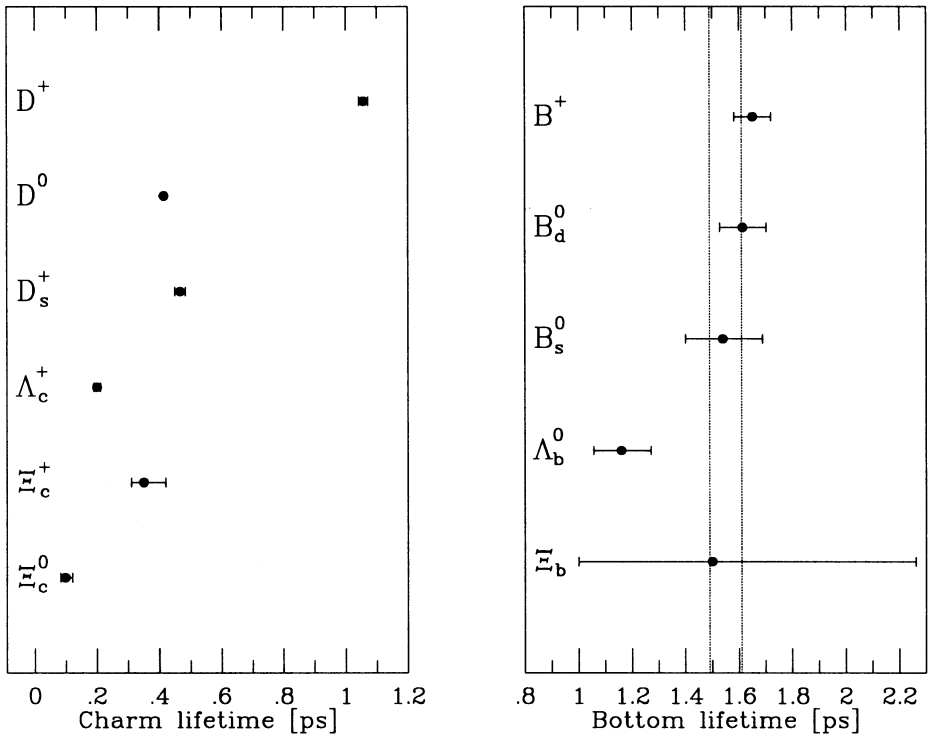


Fig. 10.3. The measured lifetimes of hadrons containing c and b quarks [3,4].

Using the measured semi-leptonic branching ratios of the D^+ and D^0, which are $17.2 \pm 1.9\%$ and $7.7 \pm 1.2\%$ respectively [3], and the measured lifetimes shown in Fig. 10.3, we can calculate the semi-leptonic widths

$$\begin{aligned} \Gamma_{\rm sl}(D^0) &= (1.22 \pm 0.20) \times 10^{-10}\ \text{MeV} \\ \Gamma_{\rm sl}(D^+) &= (1.07 \pm 0.13) \times 10^{-10}\ \text{MeV}. \end{aligned} \tag{10.13}$$

Comparing Eqs. (10.12) and (10.13) we see that the spectator model gives a fair description of the semi-leptonic decays of D mesons.

We may repeat the same exercise for the semi-leptonic decays of B mesons. The theoretical decay width is,

$$\Gamma_{\rm sl}^{(b)} = \Gamma_0(m_b) f(\frac{m_c}{m_b}) |V_{cb}|^2 \eta_0, \tag{10.14}$$

The CKM-disfavoured mode makes a negligible contribution to the total rate. Strong interaction corrections, which can be appreciable because $\alpha_S(m_b^2)$ is large, are summarized by the factor $\eta_0 \approx 0.87$ [5]. The experimental values can be obtained using the measured semi-leptonic branching ratios of the $B^\pm$ and B^0, which are $10.1 \pm 1.8 \pm 1.5\%$ and $10.9 \pm 0.7 \pm 1.1\%$ respectively [6]. When combined with the lifetimes in Fig. 10.3, the semi-

Downloaded from https://www.cambridge.org/core. UNIVERSIDAD AUTONOMA METROPOLITANA, on 17 Nov 2026 at 02:28:30, subject to the Cambridge Core terms of use, available at https://www.cambridge.org/core/terms. https://doi.org/10.1017/CBO9780511628788.011

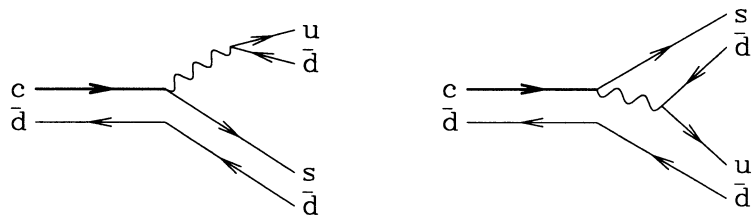


Fig. 10.4. Amplitudes contributing to D^+ decay.

leptonic widths of the B mesons are found to be

$$\begin{aligned} \Gamma_{sl}(B^0) &= (0.48 \pm 0.12) \times 10^{-10} \text{ MeV} \\ \Gamma_{sl}(B^+) &= (0.43 \pm 0.18) \times 10^{-10} \text{ MeV}. \end{aligned} \tag{10.15}$$

Eq. (10.14) can be used to determine V_{cb}. For example, choosing the values $m_b = 4.8$ GeV, $m_c = 1.4$ GeV and $V_{cb} = 0.04$ one obtains

$$\Gamma_{sl} = 2.7 \times 10^{-8} |V_{cb}|^2 \text{ MeV} = 0.44 \times 10^{-10} \text{ MeV} . \tag{10.16}$$

For further details and references to the original papers see ref. [7].

10.1.2 Hadronic decays

The simplest estimate for the total width and hence the lifetime is obtained using the spectator model. Thus, for example, in the decay of a D_s^+ meson, a non-spectator diagram would result from the annihilation of the charm quark with the anti-strange quark. This type of diagram is not considered in the spectator model. Diagrams involving spectators are suppressed by powers of the heavy quark mass, because of the small probability of overlap of the light and heavy quarks. The width in the spectator model is given simply by the weak decay of the heavy quark followed by the subsequent decay of the resulting virtual W boson.

Because of the three colours of quarks, the hadronic decay of the W to $u\bar{d}$ is three times as likely as the decay to $e\nu_e$ or $\mu\nu_\mu$, so that

$$BR(c \to eX) = \frac{1}{1+1+3} , \tag{10.17}$$

ignoring strong interaction effects. Therefore the prediction of the simplest spectator model for the total width of a charmed hadron is given by multiplying the semi-leptonic width (10.12) by five. This leads to an expected lifetime for charmed hadrons of the order of 1.2 ps. The spectator model also predicts that the lifetimes of all charmed hadrons should be the same. This prediction is not borne out by the data, as can be seen from Fig. 10.3. For example, the lifetimes of the D^+ and the D^0 mesons are very different.

Downloaded from https://www.cambridge.org/core. UNIVERSIDAD AUTONOMA METROPOLITANA, on 17 Nov 2026 at 02:28:30, subject to the Cambridge Core terms of use, available at https://www.cambridge.org/core/terms. https://doi.org/10.1017/CBO9780511628788.011

Since the semi-leptonic widths (10.13) are approximately equal, we can conclude that the failure of the spectator model is due to differences in the hadronic widths of the charmed hadrons. Many reasons can be put forward for the departures from the simple spectator model, such as non-spectator diagrams and strong radiative corrections. Fig. 10.4 shows that in the case of CKM-favoured D^+ decay there are two contributing diagrams which can interfere destructively and hence lead to a longer D^+ lifetime. However, such interference effects should be suppressed by powers of m_c, because of the small overlap of the $\bar{d}$ coming from the charm decay with the spectator $\bar{d}$. The former is initially localized in a volume of order $1/m_c^3$, whereas the latter is distributed throughout the D meson state. Since these interference effects appear to be important, we conclude that the charm quark is too light to be treated as a heavy quark in this context. Although there is a qualitative understanding of D meson decay, there is as yet no reliable quantitative description of all data on non-leptonic charm quark decays.

We obtain more encouraging results when we apply the spectator model to hadronic B hadron decays. *A priori*, one might expect the B lifetime to be a factor of $(m_c/m_b)^5$ shorter than the estimate for the charm quark lifetime given above. However this mass effect is almost entirely cancelled by the factor of $|V_{cb}|^2$ which occurs in the expression for the width. The calculation of the semi-leptonic branching ratio for B decays is complicated even in the spectator model, because of the many channels which are kinematically allowed for the decay. A detailed calculation [8] gives $BR(b \to eX) > 12.5\%$, which is compatible with the measured value.

As shown in Fig. 10.3, the ground-state hadrons containing b quarks have roughly equal lifetimes, in accordance with the spectator model[2]. Calculating the total width from the theoretical semi-leptonic width in Eq. (10.16) and the measured semi-leptonic branching ratio, we obtain a lifetime of about 1.6 ps. The measured average b lifetime [4], shown by the band in Fig. 10.3, is 1.55 ± 0.06 ps, corresponding to a proper lifetime expressed in units of length of $c\tau = 463 \pm 18$ μm. A b quark with momentum 20 GeV has a relativistic γ factor of about 4. A B meson of this momentum decaying after one lifetime will travel about 1.9 mm, which is a decay distance large enough to be measured with a particle detector. Thus the fact that V_{cb} is so small (*cf.* Eq. (10.16)) allows the measurement of separated vertices in the decays of fast moving B hadrons.

[2] Note however that the Λ_b lifetime is shorter than expected in the spectator model.

Downloaded from https://www.cambridge.org/core. UNIVERSIDAD AUTONOMA METROPOLITANA, on 17 Nov 2026 at 02:28:30, subject to the Cambridge Core terms of use, available at https://www.cambridge.org/core/terms. https://doi.org/10.1017/CBO9780511628788.011

10.2 Top quark decays

10.2.1 Conventional decays

At the Fermilab Tevatron operating at $\sqrt{s} = 1.8$ TeV about 500 $t\bar{t}$ pairs will be produced per 100 pb^{-1} of integrated luminosity. This estimate assumes that the total production cross section for a top quark of mass $m_t = 175$ GeV is about 5 pb. A more refined estimate will be given later in this chapter.

In order to identify these top quarks we must know their decay modes. We shall start by considering the decays of a free top quark in the Standard Model. Since $m_t > M_W + m_b$ a top quark decays predominantly into a b quark and an on-shell W boson

$$\begin{array}{rcl} t & \rightarrow & W^+ + b \\ & & \quad \hookrightarrow l^+ + \nu \end{array} \tag{10.18}$$

$$\begin{array}{rcl} t & \rightarrow & W^+ + b \\ & & \quad \hookrightarrow q + \bar{q} \end{array} \tag{10.19}$$

where the charged lepton, l, coming from the decay of the W can be an electron, a muon or a tau. If both top quarks decay to jets via the hadronic ($q\bar{q}$) decays of the Ws, the top quark event will be hard to identify. It is therefore usual to look for the top in channels in which one or both of the W bosons decays leptonically. The interesting final states therefore contain either a single charged lepton and jets, or two charged leptons and jets. For the latter case the background is smallest when one of the charged leptons is a muon and the other is an electron. The presence of b quarks in the final state is of great help in identifying top quark events. A b quark is tagged either by the lepton coming from its semi-leptonic decay, or by the fact that its decay products point back to a vertex displaced from the primary interaction point.

In the simplest approximation the branching ratio to leptons is given by counting the decay modes of the W, (*viz.* $e\bar{\nu}_e$, $\mu\bar{\nu}_\mu$, $\tau\bar{\nu}_\tau$ and three colours of $u\bar{d}$ and $c\bar{s}$, *cf.* Table. (8.4))

$$BR(W^+ \rightarrow e^+\bar{\nu}) = \frac{1}{3+3+3} \approx 11\%. \tag{10.20}$$

With a perfect detector the numbers of events expected at $\sqrt{s} = 1.8$ TeV per 100 pb^{-1} are

$$\begin{aligned} \mathrm{N}(e\mu + \text{jets}) &= 2 \times .11 \times .11 \times 500 \approx 12 \\ \mathrm{N}(e + \text{jets}) &= 2 \times .11 \times .66 \times 500 \approx 72. \end{aligned} \tag{10.21}$$

Downloaded from https://www.cambridge.org/core. UNIVERSIDAD AUTONOMA METROPOLITANA, on 17 Nov 2026 at 02:28:30, subject to the Cambridge Core terms of use, available at https://www.cambridge.org/core/terms. https://doi.org/10.1017/CBO9780511628788.011

The existence of both of these decay modes with the correct ratio is a first test of the decay modes of the top.

The W boson coming from top decay can be either left-handed (L) or longitudinally (0) polarized. The invariant matrix elements squared for the two processes are

$$\begin{aligned}\overline{\sum}|\mathcal{M}_L|^2 &= \frac{2G_F m_t^4}{\sqrt{2}}|V_{tb}|^2\left[2x^2(1-x^2+y^2)\right]\\ \overline{\sum}|\mathcal{M}_0|^2 &= \frac{2G_F m_t^4}{\sqrt{2}}|V_{tb}|^2\left[1-x^2-y^2(2+x^2-y^2)\right],\end{aligned} \quad (10.22)$$

where $x = M_W/m_t, y = m_b/m_t$. The result for the total width is therefore

$$\Gamma(t \to bW) = \frac{G_F m_t^3}{8\pi\sqrt{2}}|V_{tb}|^2 I(x,y), \quad (10.23)$$

where

$$I(x,y) = \left[(1-x^2)(1+2x^2) - y^2(2-x^2-y^2)\right]\lambda^{\frac{1}{2}}(1,x,y) \quad (10.24)$$

and $\lambda(a,b,c) = (a^2-(b+c)^2)(a^2-(b-c)^2)$. Keeping a non-zero b mass in the calculation of the total width leads to a correction of about 0.3%. We shall therefore neglect the b mass throughout the following discussion. In the limit $m_t \gg M_W$, we can also neglect the W mass and the total t width is given simply by

$$\Gamma(t \to bW) = \frac{G_F m_t^3}{8\pi\sqrt{2}}|V_{tb}|^2 \approx 1.76\ \text{GeV}\left(\frac{m_t}{175\ \text{GeV}}\right)^3. \quad (10.25)$$

From Eq. (10.24) the corrections to this result are of order $(M_W/m_t)^4$. In the numerical evaluation we have set $V_{tb} \approx 1$ as suggested by the unitarity relation (*cf.* Eq. (8.79))

$$|V_{tb}|^2 + |V_{cb}|^2 + |V_{ub}|^2 = 1. \quad (10.26)$$

This unitarity relation can be tested by measuring the branching fraction

$$B = \frac{\Gamma(t \to Wb)}{\Gamma(t \to Wq)}. \quad (10.27)$$

The ratio of the number of top events containing one and two tagged b jets is sensitive to this branching ratio. The first b jet signals the presence of a top event. If the tagging efficiency is known, the fraction of events which contain second b jet is a measure of the branching fraction in Eq. (10.27) and hence to V_{tb}.

The CKM-disfavoured process $t \to s$ requires knowledge of V_{ts}, which can be estimated using another unitarity relation (*cf.* Eq. (8.80))

$$V_{us}^* V_{ub} + V_{cs}^* V_{cb} + V_{ts}^* V_{tb} = 0, \quad (10.28)$$

Downloaded from https://www.cambridge.org/core. UNIVERSIDAD AUTONOMA METROPOLITANA, on 17 Nov 2026 at 02:28:30, subject to the Cambridge Core terms of use, available at https://www.cambridge.org/core/terms. https://doi.org/10.1017/CBO9780511628788.011

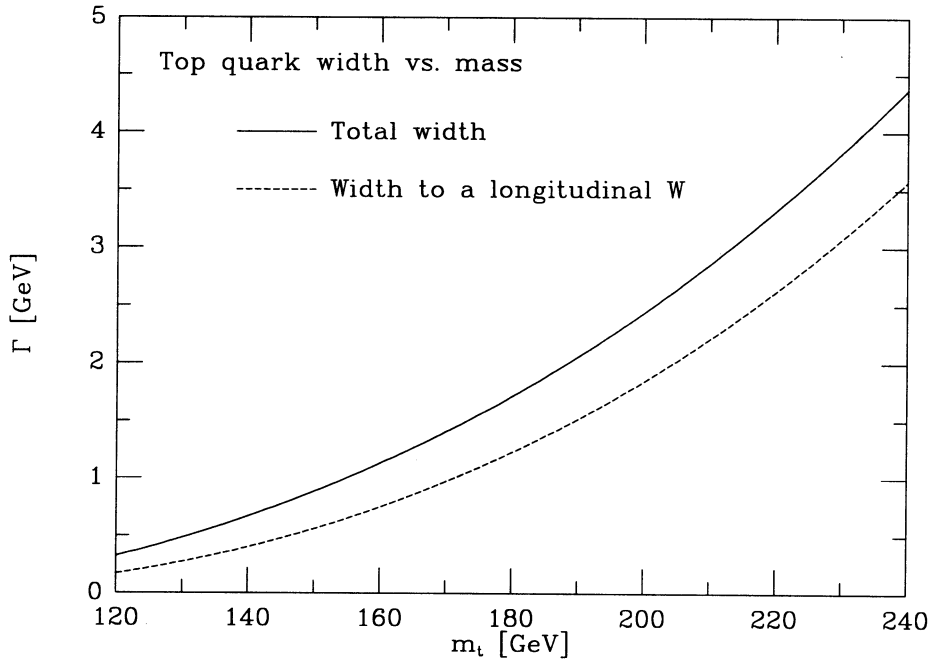


Fig. 10.5. Top quark total width and the width to a longitudinal W.

leading to $|V_{ts}| \approx |V_{cb}|$. The branching ratio into strange quarks is therefore expected to be $\sim 0.2\%$. The total width is almost identical with the width into b quarks.

Fig. 10.5 shows the width of the top quark as a function its mass. The top quark has a 'semi-weak' decay rate, *i.e.* a rate involving only one power of the Fermi constant. We therefore have a novel situation. Because of its large mass and semi-weak decay rate, the total decay width of the top quark is bigger than the typical hadronic scale. The lifetime of the top quark is only of order 10^{-25} seconds and it therefore decays before it has time to hadronize. Strong interaction effects may alter the details of final states containing top quarks but hadrons containing the top quark are not formed.

Note that the contribution of longitudinal vector bosons to the total width is a significant fraction, as shown in Fig. 10.5. Information about the longitudinal components of the vector bosons is especially significant. These components are supplied by the symmetry breaking mechanism which gives the W bosons their mass as described in Chapter 8. In the standard model the branching fraction of the top quark to longitudinal

Downloaded from https://www.cambridge.org/core. UNIVERSIDAD AUTONOMA METROPOLITANA, on 17 Nov 2026 at 02:28:30, subject to the Cambridge Core terms of use, available at https://www.cambridge.org/core/terms. https://doi.org/10.1017/CBO9780511628788.011

Ws can be calculated from Eq. (10.22). Neglecting m_b we obtain

$$\frac{\Gamma(t \to bW_0)}{\Gamma(t \to bW)} = \frac{m_t^2}{m_t^2 + 2M_W^2}. \tag{10.29}$$

It is important to check this prediction. The polarization state of the W controls the angular distribution of the leptons into which it decays. We may define the lepton helicity angle θ_e^*, which is the angle of the charged lepton in the rest frame of the W, with respect to the original direction of travel of the W (*i.e.* anti-parallel to the recoiling b quark). If the b quark jet is identified, this angle can be defined experimentally as

$$\cos\theta_e^* \approx \frac{b \cdot (e^+ - \nu)}{b \cdot (e^+ + \nu)} \approx \frac{4b \cdot e^+}{m_t^2 - M_W^2} - 1, \tag{10.30}$$

in an obvious notation where t, b, e^+ and ν represent four-momenta.

The angular distribution can be obtained by writing down the full matrix element squared for both the decay of the top and the decay of the W. This can be obtained by analogy with Eq. (10.3) after re-instating the momentum dependence and width in the W boson propagator:

$$\overline{\sum}|\mathcal{M}^{(t)}|^2 \;=\; 64G_F^2\,|V_{tb}|^2\; t \cdot e^+\; b \cdot \nu\; \frac{M_W^4}{(w^2 - M_W^2)^2 + M_W^2\Gamma_W^2}\,. \tag{10.31}$$

The four-momentum of the W boson line is denoted by $w = e^+ + \nu$. The factor coming from the W propagator is largest when the value of the invariant mass $w^2 = (e^+ + \nu)^2$ is equal to the mass of the W; the distribution becomes narrower as the total width Γ_W becomes smaller. In the narrow width approximation, Eq. (9.28), we may replace the Breit-Wigner distribution by a delta function

$$\frac{1}{(w^2 - M_W^2)^2 + M_W^2\Gamma_W^2} \approx \frac{\pi}{M_W\Gamma_W}\,\delta(w^2 - M_W^2). \tag{10.32}$$

The phase space volume element for decay into j particles,

$$d\Phi_j(P, p_1, \ldots, p_j) = (2\pi)^4\delta(P - \sum_{i=1,j} p_i) \prod_{i=1,j} \frac{d^3p_i}{2E_i(2\pi)^3}\,, \tag{10.33}$$

can be expressed recursively as the product of two-body decays. For the specific case of a three-body final state, which is of interest here, we have

$$d\Phi_3(P, p_1, p_2, p_3) = \frac{1}{2\pi}\int dp_{23}^2\, d\Phi_2(P, p_1, p_{23})\, d\Phi_2(p_{23}, p_2, p_3)\,, \tag{10.34}$$

where $p_{23} = p_2 + p_3$. Therefore the decay width is given by

$$\Gamma \;=\; \frac{1}{4\pi m_t}\int dw^2\, d\Phi_2(t, b, w)\, d\Phi_2(w, e, \nu)\, \overline{\sum}|\mathcal{M}^{(t)}|^2. \tag{10.35}$$

Downloaded from https://www.cambridge.org/core. UNIVERSIDAD AUTONOMA METROPOLITANA, on 17 Nov 2026 at 02:28:30, subject to the Cambridge Core terms of use, available at https://www.cambridge.org/core/terms. https://doi.org/10.1017/CBO9780511628788.011

In the narrow width approximation we find that Eq.(10.31) may be written using Eq. (10.30) as

$$\overline{\sum}|\mathcal{M}^{(t)}|^2 = \left[\overline{\sum}|\mathcal{M}_0|^2 \times |D_0|^2 + \overline{\sum}|\mathcal{M}_L|^2 \times |D_L|^2\right] \times \frac{\pi}{M_W \Gamma_W}\,\delta(w^2 - M_W^2). \tag{10.36}$$

Here M_0, M_L are given in Eq. (10.22) with $y = 0$ and D_0, D_L are the helicity amplitudes for the decay of a longitudinal and left-handed W boson respectively:

$$\begin{aligned} |D_0|^2 &= \frac{G_F M_W^4}{\sqrt{2}} \tfrac{1}{2} \sin^2\theta_e^* \\ |D_L|^2 &= \frac{G_F M_W^4}{\sqrt{2}} \tfrac{1}{4}(1 - \cos\theta_e^*)^2. \end{aligned} \tag{10.37}$$

We can perform the phase space integration in Eq. (10.35) using

$$d\Phi_2(P, p_1, p_2) = \frac{1}{8\pi}\frac{2|p_1|}{M_P}\frac{d\Omega}{4\pi}, \tag{10.38}$$

where p_1 is the three-momentum of the decay products in the rest-frame of the decaying particle, which has mass M_P, and $d\Omega$ is the element of solid angle. In the narrow width approximation for the W, the top width into $be\nu$ is given by the product of the width into bW and the W branching ratio into $e\nu$:

$$\Gamma(t \to be\nu) = \Gamma(t \to bW)\frac{\Gamma(W \to e\nu)}{\Gamma_W}, \tag{10.39}$$

where (*cf.* Eq. (8.92))

$$\Gamma(W \to e\nu) = \frac{G_F M_W^3}{6\sqrt{2}\pi}. \tag{10.40}$$

The normalized angular distribution of the charged leptons is therefore given by,

$$\frac{1}{N}\frac{dN(W \to e\nu)}{d\cos\theta_e^*} = \frac{3}{4(m_t^2 + 2M_W^2)}\left[m_t^2 \sin^2\theta_e^* + M_W^2(1 - \cos\theta_e^*)^2\right], \tag{10.41}$$

as shown in Fig. 10.6. A sample of 1000 tagged top events will allow a measurement of the branching fraction into longitudinal Ws with a statistical precision of 3% [9].

Downloaded from https://www.cambridge.org/core. UNIVERSIDAD AUTONOMA METROPOLITANA, on 17 Nov 2026 at 02:28:30, subject to the Cambridge Core terms of use, available at https://www.cambridge.org/core/terms. https://doi.org/10.1017/CBO9780511628788.011

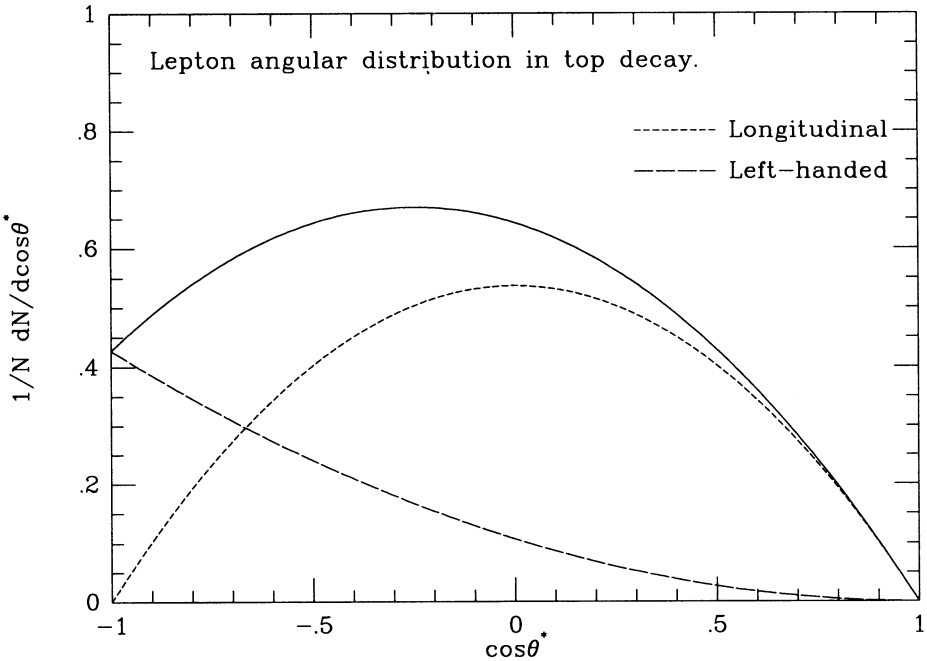


Fig. 10.6. Lepton angular distributions in top decay.

10.2.2 Unconventional decays

The experimental ratio

$$R = \frac{t\bar{t} \to e\mu + \text{jets}}{t\bar{t} \to \mu + \text{jets}} = \frac{\Gamma(t \to e + \text{jets})}{\Gamma(t \to \text{jets})} \tag{10.42}$$

gives information about the ratio of the semi-leptonic and non-leptonic widths of the top quark. In the Standard Model R is approximately one sixth. The exact value depends on the treatment of tau leptons (*e.g.* whether the leptonic decays of the τ produce a lepton which is energetic enough to be classified in the lepton sample along with the e and the μ).

It is important to look for unconventional decays of the top quark, which, if they were large enough, would give rise to a different value for the ratio R, Eq. (10.42). As an example, we consider a simple extension of the Standard Model which involves the introduction of a second Higgs doublet. Top quark decay in this model has been investigated in refs. [10,11]. In order to avoid strangeness-changing neutral currents [12] one must couple all quarks of a given charge to only one Higgs doublet. After spontaneous symmetry breaking we are left with two charged Higgs bosons $H^{\pm}$ and three neutral ones. The Lagrangian responsible for the

Downloaded from https://www.cambridge.org/core. UNIVERSIDAD AUTONOMA METROPOLITANA, on 17 Nov 2026 at 02:28:30, subject to the Cambridge Core terms of use, available at https://www.cambridge.org/core/terms. https://doi.org/10.1017/CBO9780511628788.011

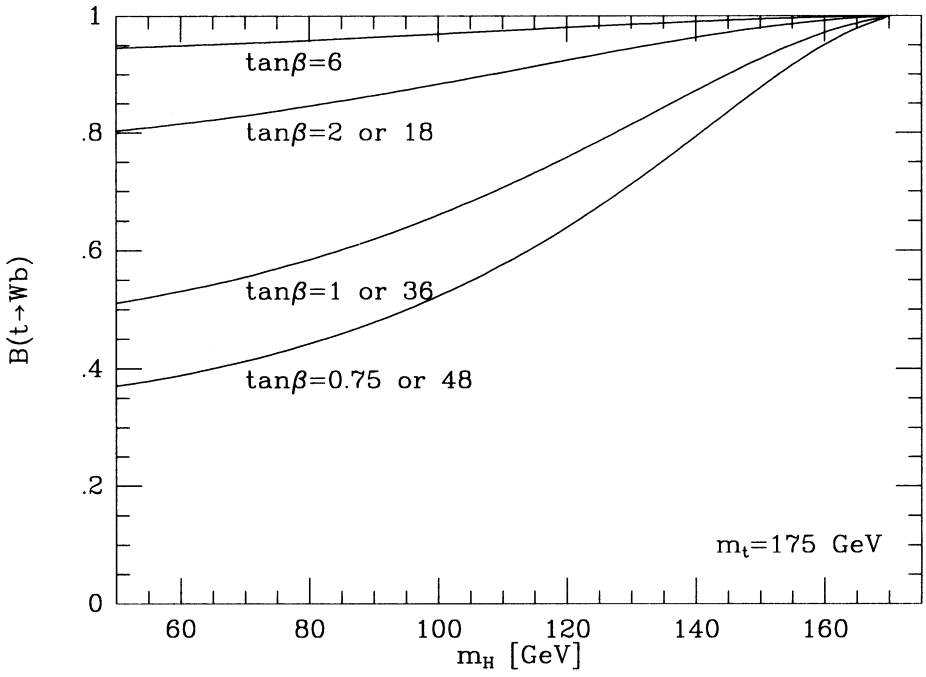


Fig. 10.7. Branching fraction to W with charged Higgs decay.

decay of the top quark contains an extra contribution given by

$$\mathcal{L} = \frac{g_W}{\sqrt{2}M_W} V_{tb} H^+ \left[m_t \cot\beta \, \bar{t}_R b_L + m_b \tan\beta \, \bar{t}_L b_R \right] , \tag{10.43}$$

where $q_{R/L} = \frac{1}{2}(1 \pm \gamma_5)q$ and $\tan\beta$ is the ratio of the vacuum expectation values of the two Higgs fields. If $M_H < m_t - m_b$, the top quark can decay to the charged Higgs boson with partial width

$$\Gamma(t \to bH^+) = \frac{G_F m_t^3}{8\pi\sqrt{2}} |V_{tb}|^2 \, J(\frac{M_H}{m_t}\frac{m_b}{m_t}, \tan\beta), \tag{10.44}$$

where

$$J(x,y,t) = \left[\left(\frac{1}{t^2} + y^2 t^2 \right)(1 + y^2 - x^2) + 4y^2 \right] \lambda^{\frac{1}{2}}(1,x,y) \, . \tag{10.45}$$

The width has a minimum for $\tan\beta = \sqrt{m_t/m_b} \sim 6$. The branching fraction $t \to Wb$ is reduced from unity by the availability of the decay to the charged Higgs boson:

$$B(t \to Wb) = \frac{\Gamma(t \to Wb)}{\Gamma(t \to Wb) + \Gamma(t \to Hb)} \, . \tag{10.46}$$

Fig. 10.7 shows the branching fraction into W bosons (10.46) as a func-

Downloaded from https://www.cambridge.org/core. UNIVERSIDAD AUTONOMA METROPOLITANA, on 17 Nov 2026 at 02:28:30, subject to the Cambridge Core terms of use, available at https://www.cambridge.org/core/terms. https://doi.org/10.1017/CBO9780511628788.011

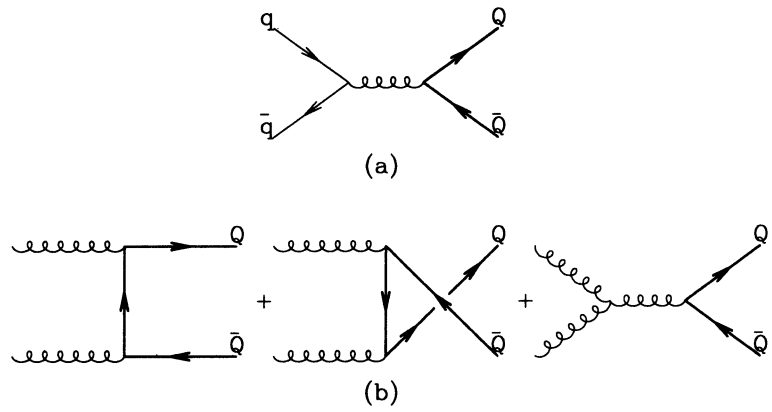


Fig. 10.8. Lowest-order Feynman diagrams for heavy quark production.

tion of the charged Higgs boson mass, for various choices of the unknown angle β.

The decay modes of the H^+ determine the signature for its detection: it should decay predominantly to $c\bar{s}$ and $\bar{\tau}\nu_\tau$, with a predominance of the former at small $\tan\beta$. If the vacuum expectation values of the two Higgs fields are taken to be equal ($\tan\beta = 1$), the branching fraction into $c\bar{s}$ is 64% and into $\bar{\tau}\nu_\tau$ is 31%.

10.3 Heavy quark production

10.3.1 Leading order

We now turn to the mechanisms by which hadrons containing heavy quarks are produced in hadronic reactions. The leading-order processes for the production of a heavy quark Q of mass m in hadron-hadron collisions are

$$\begin{aligned} &(a) \quad q(p_1) + \bar{q}(p_2) \to Q(p_3) + \overline{Q}(p_4) \\ &(b) \quad g(p_1) + g(p_2) \to Q(p_3) + \overline{Q}(p_4) \ , \end{aligned} \tag{10.47}$$

where the four-momenta of the partons are given in brackets. The Feynman diagrams which contribute to the matrix elements in $O(g^2)$ are shown in Fig. 10.8[3]. The corresponding invariant matrix elements squared [13,14] which result from the diagrams in Fig. 10.8 are given in Table 10.2. The matrix elements squared have been averaged (summed) over initial (final) colours and spins, as indicated by $\overline{\sum}$. We have introduced the following

[3] We remind the reader that $g^2 = 4\pi\alpha_S$.

Downloaded from https://www.cambridge.org/core. UNIVERSIDAD AUTONOMA METROPOLITANA, on 17 Nov 2026 at 02:28:30, subject to the Cambridge Core terms of use, available at https://www.cambridge.org/core/terms. https://doi.org/10.1017/CBO9780511628788.011

Process	$\overline{\sum}\lvert\mathcal{M}\rvert^2/g^4$
$q\,\bar{q} \to Q\,\bar{Q}$	$\frac{4}{9}\left(\tau_1^2 + \tau_2^2 + \frac{\rho}{2}\right)$
$g\,g \to Q\,\bar{Q}$	$\left(\frac{1}{6\tau_1\tau_2} - \frac{3}{8}\right)\left(\tau_1^2 + \tau_2^2 + \rho - \frac{\rho^2}{4\tau_1\tau_2}\right)$

Table 10.2. Lowest-order processes for heavy quark production. $\overline{\sum}|\mathcal{M}|^2$ is the invariant matrix element squared. The colour and spin indices are averaged (summed) over initial (final) states.

notation for the ratios of scalar products:

$$\tau_1 = \frac{2p_1.p_3}{\hat{s}}, \quad \tau_2 = \frac{2p_2.p_3}{\hat{s}}, \quad \rho = \frac{4m^2}{\hat{s}}, \quad \hat{s} = (p_1 + p_2)^2. \tag{10.48}$$

In leading order, the short-distance cross section is obtained from the invariant matrix element in the usual way:

$$d\hat{\sigma}_{ij} = \frac{1}{2\hat{s}} \frac{d^3p_3}{(2\pi)^3 2E_3} \frac{d^3p_4}{(2\pi)^3 2E_4} (2\pi)^4 \delta^4(p_1 + p_2 - p_3 - p_4) \overline{\sum} |\mathcal{M}_{ij}|^2 . \tag{10.49}$$

The first factor is the flux factor for massless incoming particles. The other terms come from the phase space for $2 \to 2$ scattering.

Consider first the hadronic differential cross section. In terms of the rapidity y, (Eq. (7.16)) and transverse momentum, p_T, the relativistically invariant phase space volume element of the final-state heavy quarks is

$$\frac{d^3p}{E} = dy\, d^2p_T . \tag{10.50}$$

Using Eqs. (7.1) and (10.49) the result for the invariant cross section may be written as

$$\frac{d\sigma}{dy_3 dy_4 d^2p_T} = \frac{1}{16\pi^2\hat{s}^2} \sum_{ij} x_1 f_i(x_1, \mu^2)\, x_2 f_j(x_2, \mu^2) \overline{\sum} |\mathcal{M}_{ij}|^2 . \tag{10.51}$$

The energy-momentum delta function in Eq. (10.49) fixes the values of x_1 and x_2 if we know the transverse momenta and rapidity of the outgoing heavy quarks. In the centre-of-mass system of the incoming hadrons we may write the components of the parton four-momenta as

$$\begin{aligned} p_1 &= \tfrac{1}{2}\sqrt{s}(x_1, 0, 0, x_1) \\ p_2 &= \tfrac{1}{2}\sqrt{s}(x_2, 0, 0, -x_2) \\ p_3 &= (m_T \cosh y_3, p_T, 0, m_T \sinh y_3) \end{aligned}$$

Downloaded from https://www.cambridge.org/core. UNIVERSIDAD AUTONOMA METROPOLITANA, on 17 Nov 2026 at 02:28:30, subject to the Cambridge Core terms of use, available at https://www.cambridge.org/core/terms. https://doi.org/10.1017/CBO9780511628788.011

$$p_4 \;=\; (m_T \cosh y_4, -p_T, 0, m_T \sinh y_4). \tag{10.52}$$

Applying energy and momentum conservation, we obtain

$$x_1 = \frac{m_T}{\sqrt{s}}(e^{y_3} + e^{y_4}), \quad x_2 = \frac{m_T}{\sqrt{s}}(e^{-y_3} + e^{-y_4}), \quad \hat{s} = 2m_T^2(1 + \cosh \Delta y). \tag{10.53}$$

The quantity $m_T = \sqrt{(m^2 + p_T^2)}$ is the transverse mass of the heavy quarks and $\Delta y = y_3 - y_4$ is the rapidity difference between them.

Using Eqs.(10.51) and (10.53), we may write the cross section for the production of a heavy quark-antiquark pair, calculated in lowest-order perturbation theory, as

$$\frac{d\sigma}{dy_3 dy_4 d^2p_T} = \frac{1}{64\pi^2 m_T^4 (1 + \cosh(\Delta y))^2} \times \sum_{ij} x_1 f_i(x_1, \mu^2)\; x_2 f_j(x_2, \mu^2) \overline{\sum} |\mathcal{M}_{ij}|^2 . \tag{10.54}$$

Expressed in terms of m, m_T and Δy, the matrix elements for the two processes in Table 10.2 are

$$\overline{\sum} |\mathcal{M}_{q\bar{q}}|^2 = \frac{4g^4}{9}\Big(\frac{1}{1 + \cosh(\Delta y)}\Big)\Big(\cosh(\Delta y) + \frac{m^2}{m_T^2}\Big)\,, \tag{10.55}$$

$$\overline{\sum} |\mathcal{M}_{gg}|^2 = \frac{g^4}{24}\Big(\frac{8\cosh(\Delta y) - 1}{1 + \cosh(\Delta y)}\Big)\Big(\cosh(\Delta y) + 2\frac{m^2}{m_T^2} - 2\frac{m^4}{m_T^4}\Big). \tag{10.56}$$

Note the form of the matrix elements squared as the rapidity separation Δy between the two heavy quarks becomes large

$$\overline{\sum} |\mathcal{M}_{q\bar{q}}|^2 \sim \text{ constant}, \quad \overline{\sum} |\mathcal{M}_{gg}|^2 \sim \exp \Delta y\,. \tag{10.57}$$

The cross section in Eq. (10.54) is therefore damped at large Δy and the dominant contribution to the total cross section comes from the region $\Delta y \leq 1$. From Eq. (10.57) we see that heavy quarks produced by light quark annihilation are more closely correlated in rapidity those produced by gluon-gluon fusion.

We shall now illustrate why it is plausible that heavy quark production should be described by perturbation theory [15]. We consider the propagators in the diagrams shown in Fig. 10.8. In terms of the above variables they can be written as

$$\begin{aligned} (p_1 + p_2)^2 = \quad 2p_1.p_2 \quad &= 2m_T^2(1 + \cosh \Delta y)\,, \\ (p_1 - p_3)^2 - m^2 = \; -2p_1.p_3 \; &= -m_T^2(1 + e^{-\Delta y})\,, \\ (p_2 - p_3)^2 - m^2 = \; -2p_2.p_3 \; &= -m_T^2(1 + e^{\Delta y})\,. \end{aligned} \tag{10.58}$$

Note that the propagators are all off-shell by a quantity of least of order m^2. It is this fact which distinguishes the production of a light quark

Downloaded from https://www.cambridge.org/core. UNIVERSIDAD AUTONOMA METROPOLITANA, on 17 Nov 2026 at 02:28:30, subject to the Cambridge Core terms of use, available at https://www.cambridge.org/core/terms. https://doi.org/10.1017/CBO9780511628788.011

from the production of a heavy quark. When a light quark is produced by these diagrams the lower cut-off on the virtuality of the propagators is provided by the light quark mass, which is less than the QCD scale Λ. Since propagators with small virtualities give the dominant contribution, the production of a light quark will not be calculable in perturbative QCD. In the production of a heavy quark, the lower cut-off is provided by the mass m. Heavy quark production is therefore controlled by α_S evaluated at the heavy quark scale.

Note also that the contribution to the cross section from values of p_T which are much greater than the quark mass is also suppressed. The differential cross section falls like $1/m_T^4$ and as m_T increases, the incoming parton flux decreases because of the increase of x_1 and x_2 according to Eq. (10.53). Since all dependence on the transverse momentum appears in the transverse mass combination, the dominant contribution to the cross section comes from transverse momenta of the order of the mass of the heavy quark.

Thus for a sufficiently heavy quark we expect the methods of perturbation theory to be applicable. It is the mass m which provides the large scale in the production. The heavy quarks have transverse momenta of the order of m and are produced close in rapidity. The production is predominantly central, because of the rapidly falling parton fluxes. Final-state interactions which transform the heavy quarks into the observed hadrons will not change the size of the cross section. A possible mechanism which might spoil this simple picture would be the interaction of the produced heavy quark with the debris of the incoming hadrons. However these interactions with spectator partons are suppressed by powers of m [16]. For large enough m they can therefore be ignored.

The theoretical arguments summarized above do not address the issue of whether the charmed quark is sufficiently heavy that the hadroproduction of charmed hadrons in all regions of phase space is well described by only processes (a) and (b) and their perturbative corrections. The applicability of these calculations to charm production will be discussed in Section 10.4.

10.3.2 Higher-order corrections

The lowest-order terms presented above are the beginning of a systematic expansion in the running coupling. For simplicity we will only discuss the radiative corrections to the total cross section. Higher-order corrections to differential cross sections have been discussed in refs. [17,18]. The

Downloaded from https://www.cambridge.org/core. UNIVERSIDAD AUTONOMA METROPOLITANA, on 17 Nov 2026 at 02:28:30, subject to the Cambridge Core terms of use, available at https://www.cambridge.org/core/terms. https://doi.org/10.1017/CBO9780511628788.011

hadronic cross section is determined as usual by

$$\sigma(P_1, P_2) = \sum_{i,j} \int dx_1 dx_2 \; f_i(x_1, \mu^2) f_j(x_2, \mu^2) \; \hat{\sigma}_{ij}(s, m^2 \mu^2) \qquad (10.59)$$

where

$$\hat{\sigma}_{ij}(s, m^2, \mu^2) = \frac{\alpha_S^2(\mu^2)}{m^2} \mathcal{F}_{ij}\left(\rho, \frac{\mu^2}{m^2}\right). \qquad (10.60)$$

Eq. (10.60) completely describes the short-distance cross section for the production of a heavy quark of mass m in terms of the functions $\mathcal{F}_{ij}$, where the indices i and j specify the types of the incoming partons. The variable μ is the renormalization and factorization scale. Its role is described later in this section. The dimensionless functions $\mathcal{F}_{ij}$ have the following perturbative expansion:

$$\mathcal{F}_{ij}\left(\rho, \frac{\mu^2}{m^2}\right) = \mathcal{F}_{ij}^{(0)}(\rho) + 4\pi\alpha_S(\mu^2)\left[\mathcal{F}_{ij}^{(1)}(\rho) + \overline{\mathcal{F}}_{ij}^{(1)}(\rho) \ln\left(\frac{\mu^2}{m^2}\right)\right] + O(\alpha_S^2) \qquad (10.61)$$

where ρ is defined in Eq. (10.48).

The lowest-order functions $\mathcal{F}_{ij}^{(0)}$ defined in Eq. (10.61) are obtained by integrating Eq. (10.49) using the results of Table 10.2. The results are

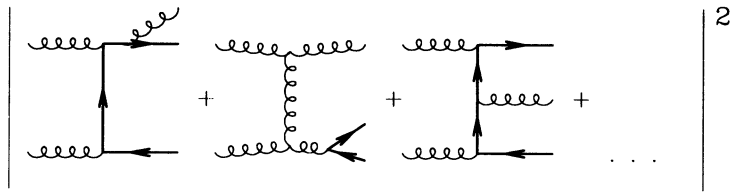
$$\begin{aligned}
\mathcal{F}_{q\bar{q}}^{(0)}(\rho) &= \frac{\pi\beta\rho}{27}\left[(2+\rho)\right], \\
\mathcal{F}_{gg}^{(0)}(\rho) &= \frac{\pi\beta\rho}{192}\left[\frac{1}{\beta}[\rho^2 + 16\rho + 16] \ln\left(\frac{1+\beta}{1-\beta}\right) - 28 - 31\rho\right], \\
\mathcal{F}_{gq}^{(0)}(\rho) &= \mathcal{F}_{g\bar{q}}^{(0)}(\rho) = 0\,,
\end{aligned} \qquad (10.62)$$

and $\beta = \sqrt{1-\rho}$. The functions $\mathcal{F}_{ij}^{(0)}$ vanish both at threshold ($\beta \to 0$) and at high energy ($\rho \to 0$). Note that the quark-gluon process is zero in lowest order, but is present in higher orders.

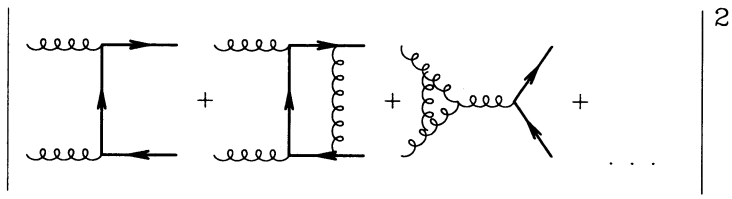
The functions $\mathcal{F}_{ij}^{(1)}$ are known [19,20]. Examples of the types of diagrams which contribute are shown in Fig. 10.9. The full calculation involves both real and virtual corrections. For full details we refer the reader to ref. [19]. In order to calculate the $\mathcal{F}_{ij}$ in perturbation theory we must perform both renormalization and factorization of mass singularities. The subtractions required for renormalization and factorization are done at mass scale μ. The dependence on μ of the next-to-leading-order term is displayed explicitly in Eq. (10.61).

As discussed in Section 7.1, μ is an unphysical parameter. The physical predictions should be invariant under changes of μ at the appropriate order in perturbation theory. If we have performed a calculation to $O(\alpha_S^3)$,

Downloaded from https://www.cambridge.org/core. UNIVERSIDAD AUTONOMA METROPOLITANA, on 17 Nov 2026 at 02:28:30, subject to the Cambridge Core terms of use, available at https://www.cambridge.org/core/terms. https://doi.org/10.1017/CBO9780511628788.011



Real emission diagrams



Virtual emission diagrams

Fig. 10.9. Examples of higher-order corrections to heavy quark production.

variations of the scale μ will lead to corrections of $O(\alpha_S^4)$,

$$\mu^2 \frac{d}{d\mu^2}\sigma = O(\alpha_S^4). \tag{10.63}$$

In this equation σ is the hadronic cross section as determined by Eq. (10.59). Using Eq. (10.63) we find that the term $\overline{\mathcal{F}}^{(1)}$, which controls the μ dependence of the higher-order perturbative contributions, is fixed in terms of the lower-order result $\mathcal{F}^{(0)}$:

$$\begin{aligned}\overline{\mathcal{F}}_{ij}^{(1)}(\rho) &= \frac{1}{8\pi^2}\Bigg[4\pi b\mathcal{F}_{ij}^{(0)}(\rho) - \int_\rho^1 dz_1 \sum_k \mathcal{F}_{kj}^{(0)}(\frac{\rho}{z_1})P_{ki}^{(0)}(z_1) \\ &\quad - \int_\rho^1 dz_2 \sum_k \mathcal{F}_{ik}^{(0)}(\frac{\rho}{z_2})P_{kj}^{(0)}(z_2)\Bigg].\end{aligned} \tag{10.64}$$

In obtaining this result we have used the renormalization group equation for the running coupling, Eq. (2.7)

$$\mu^2 \frac{d}{d\mu^2}\alpha_S(\mu^2) = -b\alpha_S^2 + \ldots \tag{10.65}$$

and the lowest-order form of the GLAP equation, Eq. (4.90)

$$\mu^2 \frac{d}{d\mu^2} f_i(x,\mu^2) = \frac{\alpha_S(\mu^2)}{2\pi}\sum_k \int_x^1 \frac{dz}{z} P_{ik}^{(0)}(z) f_k(\frac{x}{z},\mu^2) + \ldots. \tag{10.66}$$

This illustrates an important point which is a general feature of renormalization group improved perturbation series in QCD. The coefficient of the perturbative correction depends on the choice made for the scale

Downloaded from https://www.cambridge.org/core. UNIVERSIDAD AUTONOMA METROPOLITANA, on 17 Nov 2026 at 02:28:30, subject to the Cambridge Core terms of use, available at https://www.cambridge.org/core/terms. https://doi.org/10.1017/CBO9780511628788.011

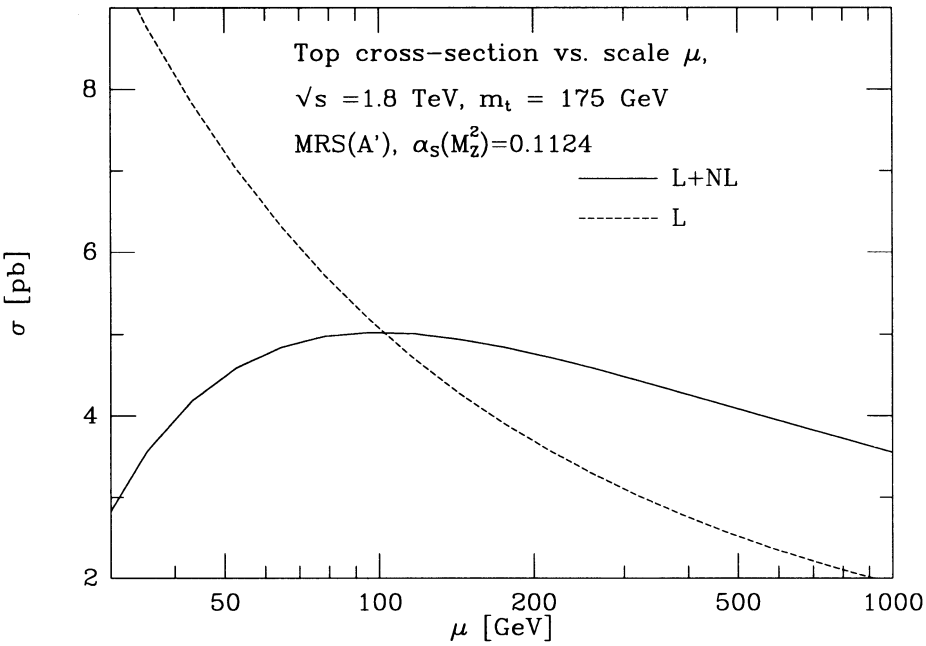


Fig. 10.10. Scale dependence of the top quark cross section in leading and next-to-leading order of perturbation theory.

μ, but the scale dependence changes the result in such a way that the physical result is independent of that choice. Thus the scale dependence is formally small because it is of higher order in α_S. This does not assure us that the scale dependence is actually *numerically* small for all series. A pronounced dependence on the scale μ is a signal of an untrustworthy perturbation series.

We elaborate on this point by showing the scale dependence found in two cases of current interest. First, in Fig. 10.10, we show the scale dependence found for the hadroproduction of a 175 GeV top quark in leading and next-to-leading order at $\sqrt{s} = 1.8$ TeV in $p\bar{p}$ collisions. The inclusion of the higher-order terms leads to a stabilization of the theoretical prediction with respect to changes in scale. The situation for the bottom quark is quite different. In Fig. 10.11 the scale dependence of the bottom quark cross section is shown. The cross section is approximately doubled by the inclusion of the higher-order corrections, which evidently do nothing to improve the stability of the prediction under changes of scale. It is apparent that the predictions for bottom production at collider energies are subject to considerable uncertainty.

We now turn to the question of flavour excitation. In the flavour excitation model the heavy quark is considered to be already present in

Downloaded from https://www.cambridge.org/core. UNIVERSIDAD AUTONOMA METROPOLITANA, on 17 Nov 2026 at 02:28:30, subject to the Cambridge Core terms of use, available at https://www.cambridge.org/core/terms. https://doi.org/10.1017/CBO9780511628788.011

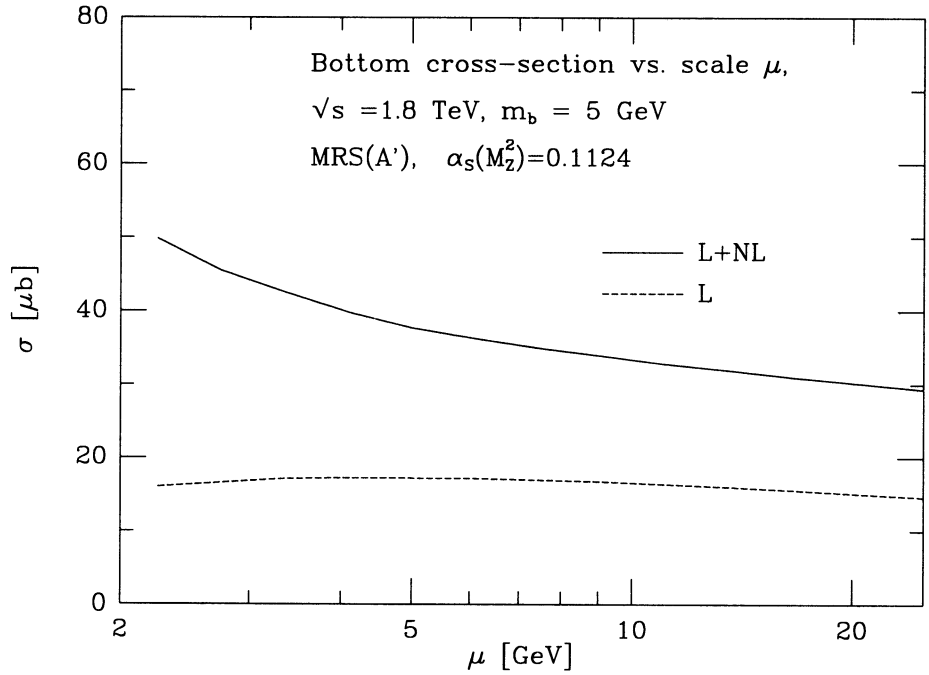
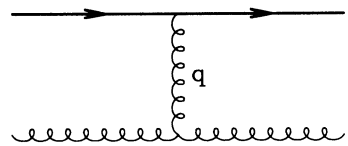


Fig. 10.11. Scale dependence of the bottom quark cross section in leading and next-to-leading order of perturbation theory.

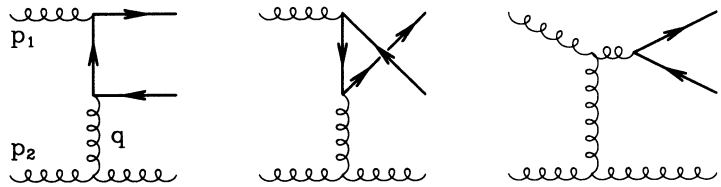
the incoming hadron. It is excited by the exchange of a gluon with the other hadron and appears on mass-shell in the final state. An example of a flavour excitation diagram is shown in Fig. 10.12(a). Note that in calculating the flavour excitation contribution the incoming heavy quark is treated as if it were on its mass-shell. If we denote the momentum transfer between the two incoming partons as q, the parton cross section will contain a factor $1/q^4$ coming from the square of the propagator of the exchanged gluon. Therefore this graph appears to be sensitive to momentum scales all the way down to the hadronic scale, (*i.e.* sensitive to low q). This casts doubt on the applicability of perturbative QCD to these processes.

We now sketch an analysis [15] which leads an important conclusion: when considering the total cross section, flavour excitation contributions should not be included. The net contribution of these diagrams is already included as a higher-order correction to the gluon-gluon fusion process. The analysis begins from the observation that the flavour excitation graph is already present as a subgraph of the first two diagrams shown in Fig. 10.12(b). Does the flavour excitation approximation accurately represent the contributions of these diagrams? In particular is the $1/q^4$ pole,

Downloaded from https://www.cambridge.org/core. UNIVERSIDAD AUTONOMA METROPOLITANA, on 17 Nov 2026 at 02:28:30, subject to the Cambridge Core terms of use, available at https://www.cambridge.org/core/terms. https://doi.org/10.1017/CBO9780511628788.011



(a) Example of flavour excitation graph



(b) Graphs containing spin–one exchange in the t–channel

Fig. 10.12. Graphs relevant for discussion of flavour excitation.

which is the signature of the presence of the flavour excitation, present in these diagrams?

We shall now indicate why the $1/q^4$ behaviour is *not* present in the sum of all three diagrams displayed in Fig. 10.12(b). In addition we shall demonstrate that the coefficient of the remaining $1/q^2$ term has the simple structure expected from QCD factorization. The remaining sensitivity to low q^2 can be factored out and absorbed in the parton distribution functions. Let us define the 'plus' and 'minus' components (also called 'light-cone' coordinates) of any vector q as follows:

$$q^+ = q^0 + q^z, \quad q^- = q^0 - q^z, \quad q^2 = q^+ q^- - q_T \cdot q_T \,. \tag{10.67}$$

We choose the upper incoming gluon in Fig. 10.12(b) to be directed along the 'plus' direction, $p_1 = p_1^+$, and the lower incoming gluon to be directed along the 'minus' direction, $p_2 = p_2^-$. We are interested in the production of heavy quarks in the 'fragmentation region' of the incoming upper gluon, far above the threshold $s \gg 4m^2$. In this region the rapidities of the produced heavy quarks are large and the q^2 of the exchanged gluon can be small, $|q^2| \ll m^2$. If the virtuality of the exchanged gluon is large, $|q^2| \geq m^2$, all the propagators of the diagrams in Fig. 10.12(b) are hard and the diagrams give rise to finite higher-order corrections. We therefore consider only the region $|q^2| \ll m^2$.

In the small-q^2 region the 'plus' component of q is small, because the

Downloaded from https://www.cambridge.org/core. UNIVERSIDAD AUTONOMA METROPOLITANA, on 17 Nov 2026 at 02:28:30, subject to the Cambridge Core terms of use, available at https://www.cambridge.org/core/terms. https://doi.org/10.1017/CBO9780511628788.011

lower final-state gluon is on-shell,

$$(p_2 - q)^2 = 0, \quad q^+ = \frac{q^2}{2p_2^-} , \tag{10.68}$$

since in the centre-of-mass system $p_1^+ = p_2^- = \sqrt{s}$. The 'minus' component of q is determined from the condition that the invariant mass of the $Q\bar{Q}$ system must be close to threshold otherwise the heavy quark propagators will become large and suppress the cross section,

$$(p_1 + q)^2 \approx 4m^2, \quad q^- \approx \frac{m^2}{p_1^+} . \tag{10.69}$$

The variable q^- is therefore also small since $p_1^+ = \sqrt{s}$. We therefore find that in the fragmentation region of the upper incoming hadron,

$$q^2 = q^+ q^- - q_T \cdot q_T \approx -q_T^2 . \tag{10.70}$$

The current J to which the exchanged gluon of momentum q couples is determined by the upper parts of the three diagrams in Fig. 10.12(b). In the fragmentation region the 'plus' component of the current J is projected out by the lower part of the diagram which, in the soft approximation, gives a factor of p_2^-. Because of the current conservation relation,

$$q^\mu J_\mu = q^+ J^- + q^- J^+ - q_T \cdot J_T = 0 , \tag{10.71}$$

which is a property of the sum of all three diagrams, we may write

$$J^+ \approx \frac{q_T \cdot J_T}{q^-} , \tag{10.72}$$

since $q^+ \ll q^-$ and $J^- \ll J^+$. Ignoring overall factors, our result for the invariant matrix element squared is given by

$$|\mathcal{M}|^2 \sim \frac{1}{x^2} \frac{|q_T \cdot J_T|^2}{q_T^4} , \tag{10.73}$$

where $x = q^-/p_2^-$. Eq. (10.73) explicitly shows that the $1/q_T^4$ behaviour is cancelled. In addition, after averaging over azimuthal directions in the transverse plane and including a flux factor $1/(2s)$ the contribution of these diagrams to the cross section may be written as

$$\sigma \sim \frac{\alpha_S C_A}{\pi} \int \frac{dq_T^2}{q_T^2} \int \frac{dx}{x} \frac{1}{2xs} \overline{\sum} |\varepsilon_T \cdot J_T|^2 . \tag{10.74}$$

The coefficient of the $1/q_T^2$ term takes the form of a low-x splitting function $\sim 1/x$, times a cross section for the scattering of gluons with transverse polarization ε_T and longitudinal momentum fraction x. It can therefore be factorized in the standard way. For further details we refer the reader

Downloaded from https://www.cambridge.org/core. UNIVERSIDAD AUTONOMA METROPOLITANA, on 17 Nov 2026 at 02:28:30, subject to the Cambridge Core terms of use, available at https://www.cambridge.org/core/terms. https://doi.org/10.1017/CBO9780511628788.011

to ref. [15]. The calculation of ref. [19] provides an explicit verification of this cancellation in the total cross section.

10.4 Charm and bottom quark production

In this section we will compare the next-to-leading theory outlined above to experimental data on bottom and charm production. For the purposes of this comparison it is important to assess the theoretical errors on the cross section prediction, which can be as large as the experimental errors. The value of the heavy quark mass m is the principal parameter controlling the size of the cross section. The m dependence is much more marked than the $1/m^2$ dependence in the short-distance cross section expected from Eq. (10.60). As the mass decreases, the values of x at which the parton distributions are evaluated become smaller (*cf.* Eq. (10.53)) and the cross section rises because of the growth of the parton flux.

The approach which we shall take to the estimate of theoretical errors in heavy quark cross sections is taken from refs. [21,22]. We shall take the charm and bottom masses to lie in the ranges

$$\begin{aligned} 1.2 &< m_c < 1.8 \text{ GeV} \\ 4.5 &< m_b < 5.0 \text{ GeV}. \end{aligned} \tag{10.75}$$

A second important parameter is the value of the strong coupling. The value of α_S is fixed by the fitting procedure which determines the parton distributions and is correlated with the form of the gluon distribution. However, to be conservative, it is customary to consider a slightly larger range of Λ than fixed by the parton distribution fits. An overall view of the uncertainty in α_S is given in Chapter 12. In this chapter we just present the range of five flavour Λ used in the plots without comment. For fixed-target charm and bottom hadroproduction by pions the range is

$$60 \text{ MeV} < \Lambda_{\overline{\text{MS}}}(5) < 204 \text{ MeV}\,, \tag{10.76}$$

with corresponding variations of the nucleon structure functions [23]. The pion distributions functions are from ref. [24]. We shall arbitrarily choose to vary the scale parameter μ in the range $m/2 < \mu < 2m$ to test the sensitivity to μ. We shall consider the extremum of all these variations to give an estimate of the theoretical error.

We immediately encounter a difficulty with this procedure in the case of charm. Variations of μ down to $m/2$ will carry us into the region $\mu <$ 1 GeV in which we certainly do not trust perturbation theory. A estimate of the theoretical error on charm production cross sections in this way is

Downloaded from https://www.cambridge.org/core. UNIVERSIDAD AUTONOMA METROPOLITANA, on 17 Nov 2026 at 02:28:30, subject to the Cambridge Core terms of use, available at https://www.cambridge.org/core/terms. https://doi.org/10.1017/CBO9780511628788.011

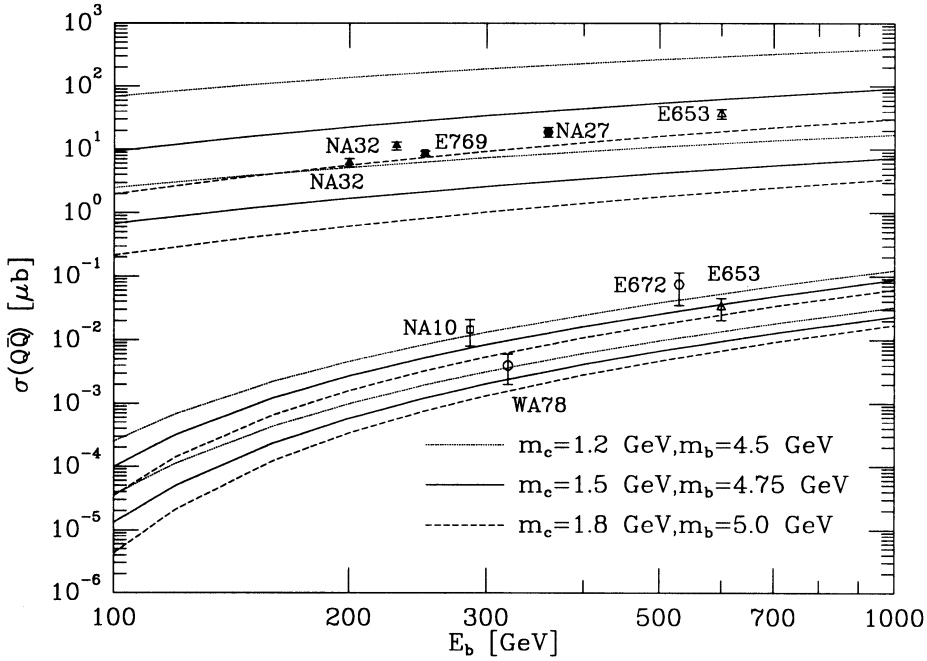


Fig. 10.13. Data on pion hadroproduction of $c\bar{c}$ and $b\bar{b}$ *vs.* beam energy compared with theory. Adapted from ref. [22].

therefore not possible. In calculating the curves for charm production the lower limit on the factorization scale is taken to be $\mu_F = 2m_c$.

The dependence on the value chosen for the heavy quark mass is particularly acute for the case of charm production. In fact, variations due to plausible changes in the quark mass, Eq. (10.75), are bigger than the uncertainties due to variations in the other parameters. We shall therefore take the aim of studies of the hadroproduction and photoproduction of charm to be the search for an answer to the following question: Is there a reasonable value for the charm quark mass which can accommodate the majority of the data?

In Fig. 10.13, adapted from ref. [22], we show the theoretical prediction for charm and bottom production using pion beams. Note the scale of the figure and the large spread in the theoretical predictions. Also plotted is a compilation of data. For the references to the original data we refer the reader to ref. [22]. We see that a value of $m_c = 1.5$ GeV gives a fair description of the data on the hadroproduction of charm. After inclusion of the $O(\alpha_S^3)$ corrections, the data can be explained without recourse to very small values of the charmed quark mass.

This conclusion is further reinforced by consideration of the data on

Downloaded from https://www.cambridge.org/core. UNIVERSIDAD AUTONOMA METROPOLITANA, on 17 Nov 2026 at 02:28:30, subject to the Cambridge Core terms of use, available at https://www.cambridge.org/core/terms. https://doi.org/10.1017/CBO9780511628788.011

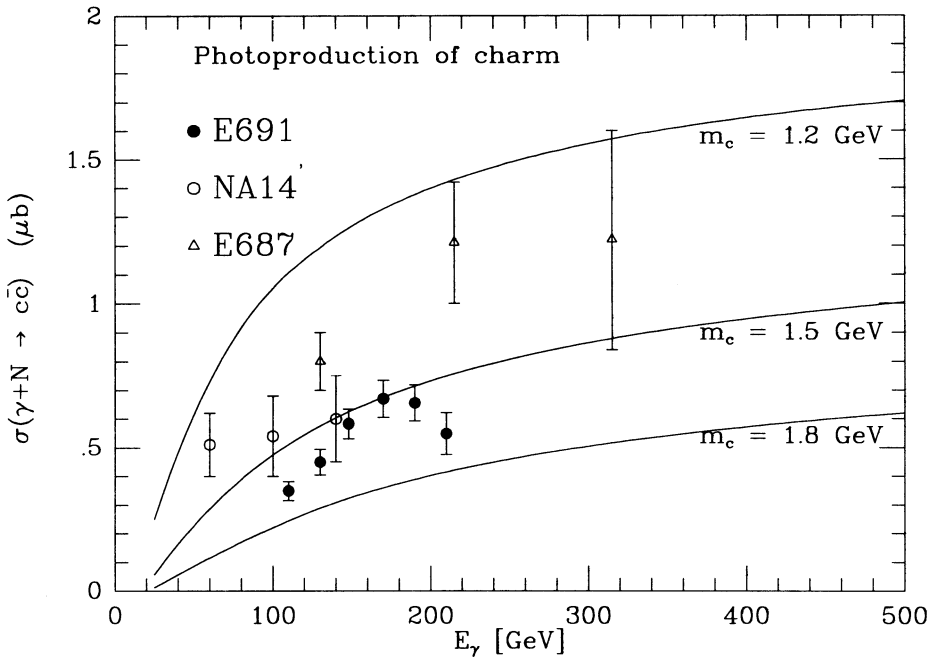


Fig. 10.14. Data on photoproduction of charm compared with theoretical lower limits [29].

photoproduction of charm. The higher-order $O(\alpha\alpha_S^2)$ corrections to photoproduction have been considered in ref. [25]. After inclusion of these higher-order terms we obtain predictions for the total cross section as a function of the energy of the photon beam. The principal uncertainty comes from the value of the heavy quark mass, so we have plotted the minimum cross section which is obtained by varying Λ in the range

$$90 \text{ MeV} < \Lambda_{\overline{\text{MS}}}(5) < 250 \text{ MeV} , \tag{10.77}$$

and the scale μ within the range 1 GeV $< \mu < 2m$ for three values of the charm quark mass. The comparison with the data on the photoproduction of charm [26,27,28], shown in Fig. 10.14, indicates that charm quark masses smaller than 1.5 GeV are not needed to give an acceptable explanation of the data.

In conclusion, within the large uncertainties present in the theoretical estimates, modern data on the production of charm can be explained with a charm quark mass of the order of 1.5 GeV. This is not true of all data on the hadroproduction of charm, especially the older experiments. For a review of the older experimental situation we refer the reader to ref. [30]. Much information is also available on the x_F and p_T distributions of charmed hadrons, as well as data on the correlations between the

Downloaded from https://www.cambridge.org/core. UNIVERSIDAD AUTONOMA METROPOLITANA, on 17 Nov 2026 at 02:28:30, subject to the Cambridge Core terms of use, available at https://www.cambridge.org/core/terms. https://doi.org/10.1017/CBO9780511628788.011

produced heavy quark and antiquark. For a comparison of these data with theoretical predictions we refer the reader to ref. [22].

At fixed-target energies the cross section for the production of bottom quarks is theoretically more reliable. The scale dependence plot has a characteristic form similar to Fig. 10.10 and it is possible to make estimates of the theoretical errors. The comparison with data on the production of bottom in pion beams at fixed-target energies is shown in Fig. 10.13.

As emphasized above, the theoretical prediction for bottom quark production at collider energies is very uncertain. The cause of this large uncertainty is principally the very small value of x at which the parton distributions are probed. In fact, at present collider energies, ($\sqrt{s} = 1.8$ TeV), the bottom cross section is sensitive to the gluon distribution function at values of $x < 10^{-2}$. Measurements of the gluon distribution function [31] at such small values of x are not very precise and this leads to an uncertainty in the cross section. An associated problem is the form of the short-distance cross section in the large $\hat{s}$ region. From Eq. (10.62) we see that lowest-order short-distance cross sections, $\mathcal{F}^{(0)}$, tend to zero in the large $\hat{s}$ region. This is a consequence of the fact that they involve at most spin-$\frac{1}{2}$ exchange in the t-channel, as shown in Fig. 10.8. The higher-order corrections to the gg and gq processes have a different behaviour because they involve spin-1 exchange in the t-channel. The relevant diagrams for the gg process are shown in Fig. 10.12(b). In the high energy limit they yield a constant cross section, independent of energy [19]. Naturally these high-$\hat{s}$ contributions are damped by the small number of energetic gluons in the parton flux, but at collider energies the region $\sqrt{\hat{s}} \gg m$ makes a sizeable contribution to the bottom cross section. The fact that this constant behaviour is present in both $\mathcal{F}^{(1)}$ and $\overline{\mathcal{F}}^{(1)}$ defined in Eq. (10.61) indicates the sensitivity of the size of this term to the value chosen for μ. There is therefore an interplay between the size of this term and the small-x behaviour of the gluon distribution function.

The calculations of ref. [19] also allow us to examine the p_T and rapidity distributions of the one heavy quark inclusive cross section, $p\bar{p} \to b + X$. Although the prediction of the total bottom cross section at collider energy is uncertain, it is plausible that the shape of the transverse momentum and rapidity distributions is well described by the form found in lowest-order perturbation theory. The supporting evidence for this conjecture is shown in Fig. 10.15, which demonstrates that the inclusion of the first non-leading correction does not significantly modify the shape of the transverse momentum and rapidity distributions. At a fixed value of μ, the two curves lie on top of one another if the lowest order is multiplied by a constant factor. Similar results hold also for the shape of the top quark distribution [17].

Downloaded from https://www.cambridge.org/core. UNIVERSIDAD AUTONOMA METROPOLITANA, on 17 Nov 2026 at 02:28:30, subject to the Cambridge Core terms of use, available at https://www.cambridge.org/core/terms. https://doi.org/10.1017/CBO9780511628788.011

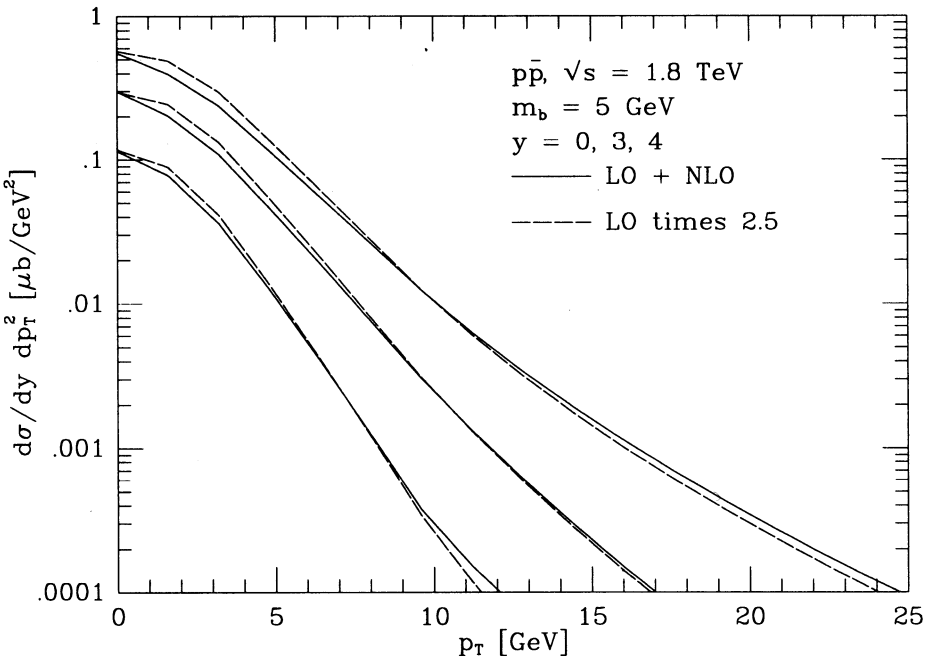


Fig. 10.15. The shape of the p_T distribution for bottom quark production. Figure from ref. [17].

The UA1 collaboration have investigated the transverse momentum distribution of the produced bottom quarks [32]. In Fig. 10.16 a comparison of UA1 data with the full α_S^3 prediction is made. The data are plotted as a function of the lower cut-off $p_T^b(\text{min})$ on the transverse momentum of the b quark. The theoretical curves [22] are predictions for the production of b quarks. The data have been corrected for the fragmentation of a b quark into a B hadron and hence can be compared directly with the theoretical prediction. The cross section at the Born level is $O(\alpha_S^2)$ so there is evidently a considerable sensitivity in the theoretical prediction to the value chosen α_S (or for Λ). The range of five-flavour Λ in the $\overline{\text{MS}}$ scheme is chosen in order to cover both the preferred value of deep inelastic scattering, ($\Lambda \approx 150$ MeV) and the value preferred by experiments at the Z-pole, ($\Lambda \approx 300$ MeV). The match between experiment and these values of Λ can be checked by referring back to Fig. 2.5. The agreement between experiment and theory in Fig. 10.16 is satisfactory.

The corresponding prediction for the p_T dependence of the bottom production cross section at the Tevatron is shown in Fig. 10.17, compared with data from the CDF and D0 collaborations, obtained using various methods to detect the b quarks. The data tend to lie on the high side

Downloaded from https://www.cambridge.org/core. UNIVERSIDAD AUTONOMA METROPOLITANA, on 17 Nov 2026 at 02:28:30, subject to the Cambridge Core terms of use, available at https://www.cambridge.org/core/terms. https://doi.org/10.1017/CBO9780511628788.011

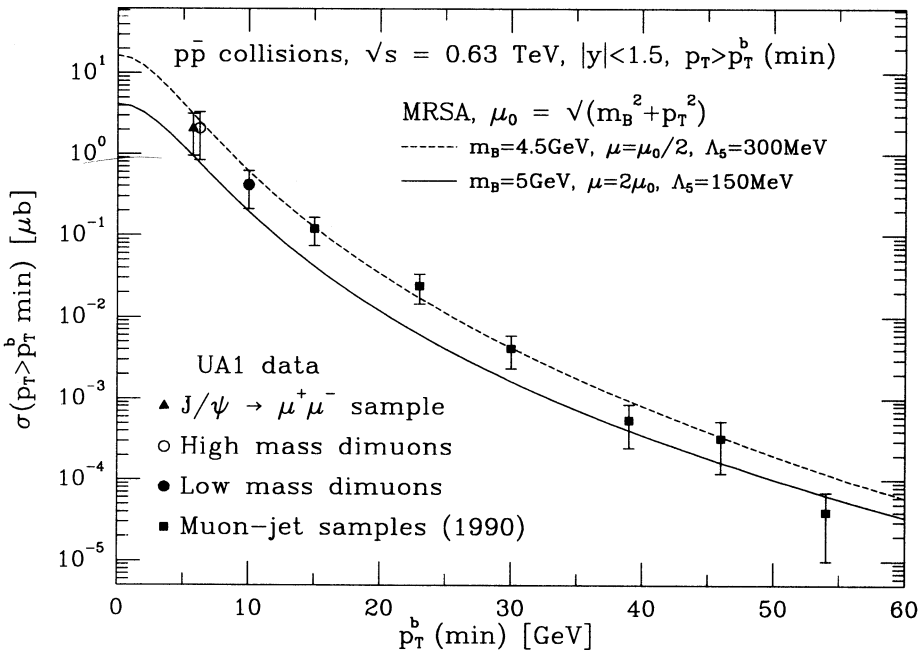


Fig. 10.16. The cross section for bottom quark production at CERN [32].

of the theoretical prediction. Resummation of small x effects [35] may lead to a further enhancement of the theoretical prediction, perhaps by about 30%. In view of the large theoretical uncertainties, the agreement between theory and experiment can be considered satisfactory.

10.5 Top quark production

The belief that the top quark had to exist was based both on theoretical and experimental evidence. The theoretical motivation is that complete families are required for the cancellation of anomalies in the currents which couple to gauge fields. Hence as explained in Section 8.3 the partner of the b, τ and ν_τ was needed to complete the third family.

An experimental reason to believe in the existence of the top quark was the determination of the weak isospin of the bottom quark by e^+e^- annihilation experiments. The produced b and $\bar{b}$ quarks are identified either by looking for displaced vertices or by looking for leptons which have a large p_T relative to the jet axis. As may be seen from Eq. (3.1), the forward-backward asymmetry of b jets in e^+e^- annihilation at the Z

Downloaded from https://www.cambridge.org/core. UNIVERSIDAD AUTONOMA METROPOLITANA, on 17 Nov 2026 at 02:28:30, subject to the Cambridge Core terms of use, available at https://www.cambridge.org/core/terms. https://doi.org/10.1017/CBO9780511628788.011

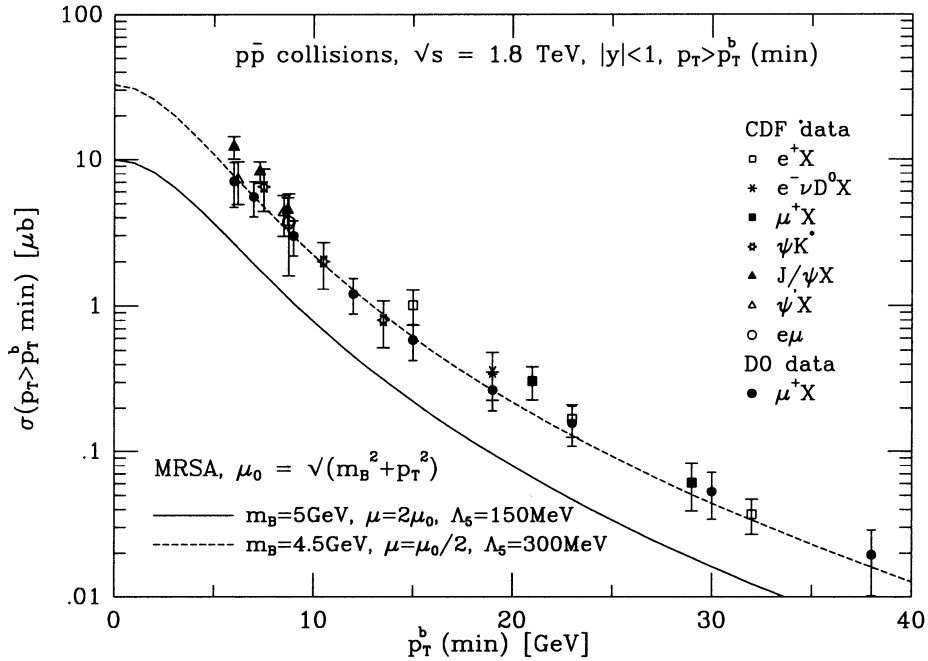


Fig. 10.17. The cross section for bottom quark production at Fermilab [33,34].

resonance is controlled by couplings to the electron and the b quark,

$$A_{FB}(b) = \frac{3}{4}\frac{2V_eA_e}{V_e^2+A_e^2}\frac{2V_bA_b}{V_b^2+A_b^2}\,. \tag{10.78}$$

On the other hand from Eq. (8.91) the total width of the Z into b quarks is given by

$$\Gamma(Z\to b\bar{b}) = \frac{G_F M_Z^3}{2\sqrt{2}\pi}(V_b^2+A_b^2)\,. \tag{10.79}$$

Taking the couplings to the electron to have their standard values, these two measurements are sufficient to measure the left- and right-handed weak isospin of the b quark. An early determination of the couplings of the b quark (before the discovery of the top) gave the values [36],

$$T^3(b_L) = -0.490^{+0.015}_{-0.012},\quad T^3(b_R) = -0.028\pm 0.056\,. \tag{10.80}$$

The simplest hypothesis is therefore that the left-handed bottom quark is in an SU(2) doublet with the top quark, although more complicated schemes are certainly possible. More precise values of the couplings of the b quark are now available [37,38]. It is less interesting to express them as constraints on the weak isospin of the b quark since the discovery of the t quark.

Downloaded from https://www.cambridge.org/core. UNIVERSIDAD AUTONOMA METROPOLITANA, on 17 Nov 2026 at 02:28:30, subject to the Cambridge Core terms of use, available at https://www.cambridge.org/core/terms. https://doi.org/10.1017/CBO9780511628788.011

	m_t [GeV]	σ [pb]
CDF	$175.6 \pm 5.7(\text{stat}) \pm 7.4(\text{sys})$	$7.5^{+1.6}_{-1.6}$
D0	$170 \pm 15(\text{stat}) \pm 10(\text{sys})$	$5.2^{+1.8}_{-1.8}$

Table 10.3. Current results for top quark production from Fermilab [41,42].

Indirect constraints on the mass of the top quark are obtained from precision electroweak measurements, such as the W mass measurement. As described in Section 8.2.2 the top mass leads to observable effects on the ρ parameter. The current limits on the top quark mass from precision electroweak measurements are [38]

$$m_t = 178^{+8+17}_{-8-20}\ \text{GeV}\,. \tag{10.81}$$

The value extracted for the top quark mass has a mild dependence on the mass of the Higgs boson. The central value is extracted for $M_H = 300$ GeV. The second error corresponds to varying the Higgs boson mass in the range 60 GeV $< M_H <$ 1 TeV.

The first direct evidence for the top quark was the observation of its production in $p\bar{p}$ collisions at Fermilab [39,40]. The current results from the two collaborations [41,42] based on about 100 pb^{-1} per experiment at $\sqrt{s} = 1.8$ TeV are given in Table 10.3. Note that the measured cross sections are extremely small. Indeed with the measured cross sections one predicts that only about 1300 $t\bar{t}$ pairs have been produced at Fermilab. The actual number of events observed is further reduced by the branching ratios to observable modes and by experimental acceptances and efficiencies. It should be noted that the top quark mass is still quite uncertain. In the following sections we will discuss the comparison of the experimental results with theory, using a nominal value of 175 GeV.

10.5.1 Top cross section

The expected cross section for the process

$$p + \bar{p} \to t + \bar{t} + X \tag{10.82}$$

is shown in Fig. 10.18 as a function of the top mass at $\sqrt{s} = 1.8$ and 2 TeV. The errors on the theoretical prediction will be discussed below. The cross section is calculated using next-to-leading-order QCD. Also plotted are the results at $\sqrt{s} = 1.8$ TeV of the CDF and D0 collaborations at the time of writing. As discussed above, the top quark cross section is calculable in perturbation theory because $m_t \gg \Lambda$. This condition is certainly valid for the case of the top quark and suggests that its production cross

Downloaded from https://www.cambridge.org/core. UNIVERSIDAD AUTONOMA METROPOLITANA, on 17 Nov 2026 at 02:28:30, subject to the Cambridge Core terms of use, available at https://www.cambridge.org/core/terms. https://doi.org/10.1017/CBO9780511628788.011

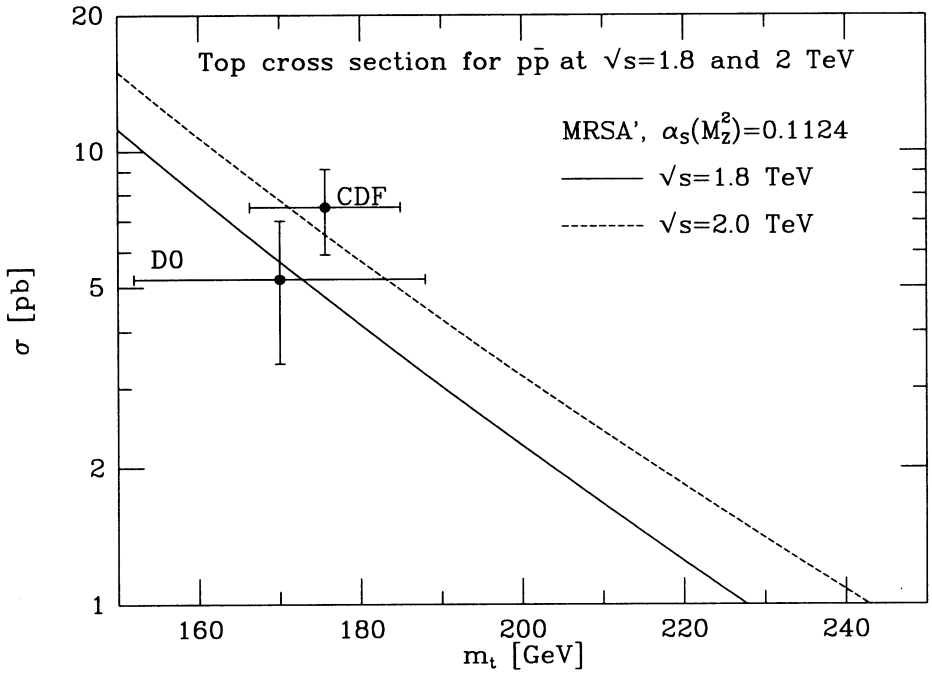


Fig. 10.18. The cross section for top quark production versus m_t.

section should be well determined. Next-to-leading order corrections to the $q\bar{q}$ process are found to be moderate, with the bulk of the correction occurring near threshold. Corrections to the gg process are large, both at threshold and at high energy.

The relative importance of the various kinematic regions is determined by the parton luminosity defined in Eq. (7.12):

$$\frac{dL_{ij}}{d\ln\tau} = \frac{1}{1+\delta_{ij}} \int_0^1 dx_1 dx_2 \times \Big[(x_1 f_i^A(x_1,\mu^2)\; x_2 f_j^B(x_2,\mu^2)) + (1 \leftrightarrow 2) \Big] \delta(\tau - x_1 x_2) \quad (10.83)$$

where f_i^A is the density of partons of type i in hadron A. In terms of these parton fluxes the hadronic cross-section is given by

$$\frac{d\sigma(s)}{\ln\tau} = \frac{\alpha_S^2(\mu^2)}{2m^2} \sum_{i,j} \frac{dL_{ij}(\tau,\mu)}{d\ln\tau} \mathcal{F}_{ij}\left(\frac{\rho^H}{\tau}, \frac{\mu^2}{m^2}\right) . \quad (10.84)$$

Fig. 10.19 shows that at $\sqrt{s} = 1.8$ TeV, the top quark is produced predominantly by $q\bar{q}$ annihilation, with large corrections near threshold. For $m = 175$ GeV, about 90% of the cross section is due to $q\bar{q}$ annihilation. This implies that calculations of the cross section should be quite reliable,

Downloaded from https://www.cambridge.org/core. UNIVERSIDAD AUTONOMA METROPOLITANA, on 17 Nov 2026 at 02:28:30, subject to the Cambridge Core terms of use, available at https://www.cambridge.org/core/terms. https://doi.org/10.1017/CBO9780511628788.011

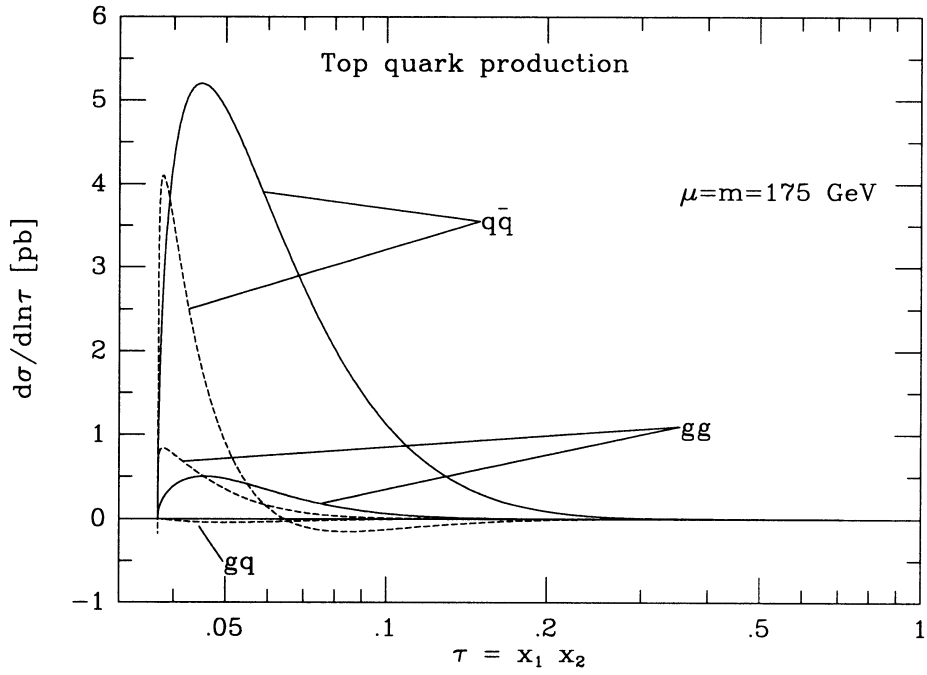


Fig. 10.19. $O(\alpha_S^2)$ curves (solid) and $O(\alpha_S^3)$ curves (dashed).

because they depend on well-measured quark distribution functions.

Near threshold ($\beta \to 0$), the results for the functions $\mathcal{F}_{ij}^{(0,1)}$ defined in Eq. (10.61) are

$$\mathcal{F}_{q\bar{q}}^{(1)} \to \mathcal{N}_{q\bar{q}}\left[-\frac{\pi^2}{6}+\beta\left(\frac{16}{3}\ln^2(8\beta^2)-\frac{82}{3}\ln(8\beta^2)\right)\right]$$
$$\mathcal{F}_{gg}^{(1)} \to \mathcal{N}_{gg}\left[\frac{11\pi^2}{42}+\beta\left(12\ln^2(8\beta^2)-\frac{366}{7}\ln(8\beta^2)\right)\right] \quad (10.85)$$

and $\mathcal{F}_{q\bar{q}}^{(0)}, \mathcal{F}_{gq}^{(1)} \to O(\beta)$. The normalization constants are defined by

$$\mathcal{N}_{ij}=\frac{1}{8\pi^2}\frac{\mathcal{F}_{ij}^{(0)}}{\beta},\quad \mathcal{N}_{q\bar{q}}=\frac{1}{72\pi},\quad \mathcal{N}_{gg}=\frac{7}{1536\pi}\,. \quad (10.86)$$

The rapid rise of the cross section near threshold displayed in Fig. 10.19 is due to the logarithmic terms in Eq. (10.85). These corrections are larger for smaller top quark mass, when gluon-gluon processes are more important. The constant behaviour of the cross section near threshold is a consequence of the Coulomb singularity. This effect is repulsive in the dominant $q\bar{q}$ octet channel. The correction due to this effect is small; after resumming the Coulomb terms it is found that additional correction

Downloaded from https://www.cambridge.org/core. UNIVERSIDAD AUTONOMA METROPOLITANA, on 17 Nov 2026 at 02:28:30, subject to the Cambridge Core terms of use, available at https://www.cambridge.org/core/terms. https://doi.org/10.1017/CBO9780511628788.011

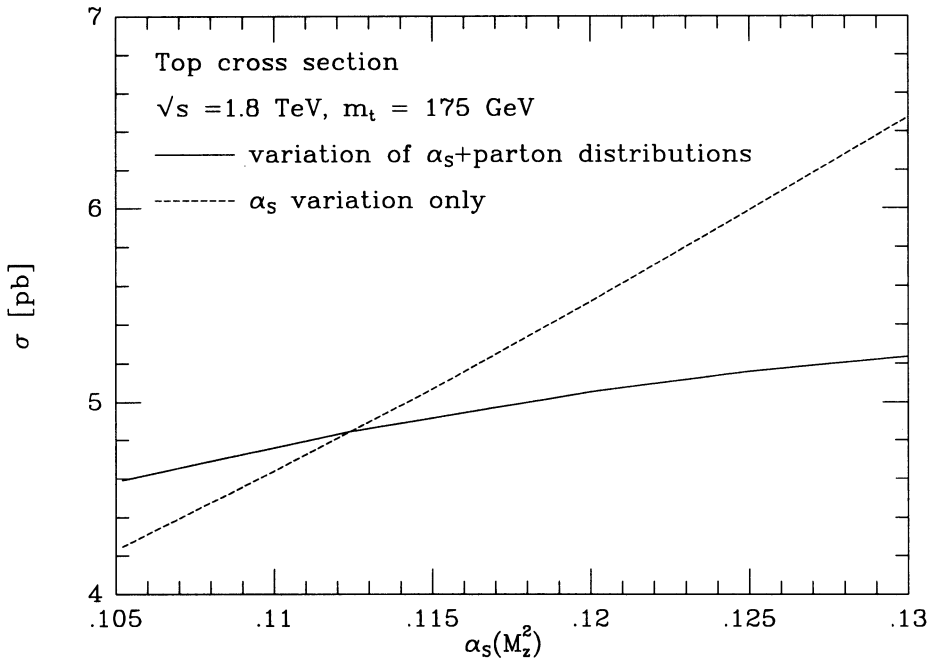


Fig. 10.20. The cross section for top quark production versus $\alpha_S(M_Z^2)$. Adapted from ref. [44].

to the cross section not included in the next-to-leading order calculation is less than one percent, in part because of cancellation between gg and $q\bar{q}$ channels [43,44].

We now turn to numerical estimates. Earlier estimates are given in [44-48]. The input parameters which we have to specify are the form of the parton distributions, the value of α_S and the value of the renormalization and factorization scale, μ. For the MRS(A′) distribution, $\alpha_S(M_Z^2) = 0.1124$, the result for $m_t = 175$ GeV and $\mu = m_t$ is $\sigma = 4.84$ pb. The sensitivity to the form of the parton distribution functions is quite small mainly because the top quark is predominantly produced by the well-measured quark distributions. The effect of the α_S uncertainty is more important. Increasing α_S without changing the parton distributions gives the dashed curve in Fig. 10.20. This calculation of the dependence on α_S is an overestimate since it does not take into account the increased shrinkage of the quark distribution functions for larger α_S in the evolution from lower energy where they are measured [48]. Fig. 10.20 shows the predicted value of the top cross section using parton distribution functions [49] which have been fitted with different fixed values of α_S. The overall dependence of the cross section on the value of α_S is quite small. We

Downloaded from https://www.cambridge.org/core. UNIVERSIDAD AUTONOMA METROPOLITANA, on 17 Nov 2026 at 02:28:30, subject to the Cambridge Core terms of use, available at https://www.cambridge.org/core/terms. https://doi.org/10.1017/CBO9780511628788.011

estimate the errors in the cross section by taking $0.105 < \alpha_S(M_Z^2) < 0.130$ and $m_t/2 < \mu < 2m_t$ and find that at a fixed top mass the cross section is unlikely to be uncertain by more than $\pm 15\%$. The final result for the top quark cross section is

$$\sigma(m_t = 175 \text{ GeV}) = 4.84^{+0.73}_{-0.69} \text{ pb}. \tag{10.87}$$

The cross sections quoted above are given in the narrow width approximation.

10.5.2 Prospects for top studies

As noted in the previous section, the cross section for $t\bar{t}$ production at the Tevatron collider is extremely small. Therefore in order to study the top quark in more detail it is necessary to increase either the energy or the luminosity of the collider (or both).

The next collider run at the Fermilab Tevatron is scheduled for 1999 after completion of the Main Injector project. The energy will be increased to $\sqrt{s} = 2$ TeV and the luminosity will increase to about 40 pb^{-1} per week from the present value of 4 pb^{-1} per week. For $m_t = 175$ GeV the higher energy increases the $t\bar{t}$ cross section by about 37% relative to its value at $\sqrt{s} = 1.8$ TeV.

Therefore in the early years of the next century one will have data samples in $p\bar{p}$ annihilation at $\sqrt{s} = 2$ TeV measured in inverse femtobarns. The constraints on the Standard Electroweak Model from the top quark and W mass measurements which will be possible with these data can be seen in Fig. 10.21, calculated using ref. [50]. The band of values at each value of the Higgs boson mass corresponds to the uncertainty on the value of the electromagnetic fine structure constant at the Z mass [51]

$$[\alpha(M_Z^2)]^{-1} = 128.89 \pm 0.09. \tag{10.88}$$

With 2 fb^{-1} of data, CDF estimate measurement errors of $\delta M_W = 40$ MeV and $\delta m_t = 4$ GeV [52].

As shown in Fig. 10.22, the expected cross section in pp interactions at 14 TeV is

$$\sigma = 785^{+300}_{-130} \text{ pb}. \tag{10.89}$$

This is more than a factor of one hundred larger than the cross section at the Tevatron, primarily due to the large flux of incoming gluons. More 90% of the cross section at the LHC is due to processes with incoming gluons. Therefore at a luminosity of 10^{34} cm^{-2} s^{-1} we expect about seven top quark pairs produced per second. The large cross section and luminosity will make the LHC a powerful machine to study the top quark.

Downloaded from https://www.cambridge.org/core. UNIVERSIDAD AUTONOMA METROPOLITANA, on 17 Nov 2026 at 02:28:30, subject to the Cambridge Core terms of use, available at https://www.cambridge.org/core/terms. https://doi.org/10.1017/CBO9780511628788.011

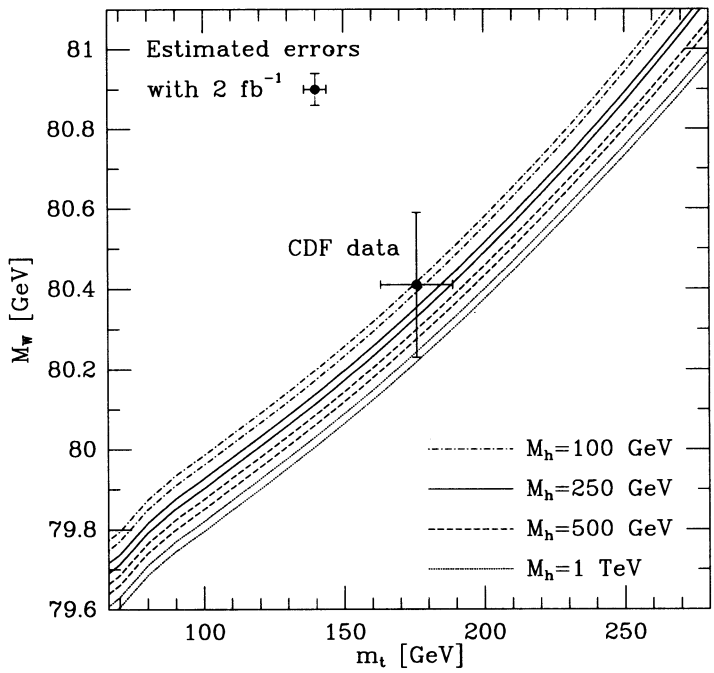


Fig. 10.21. Testing the Standard Electroweak Model.

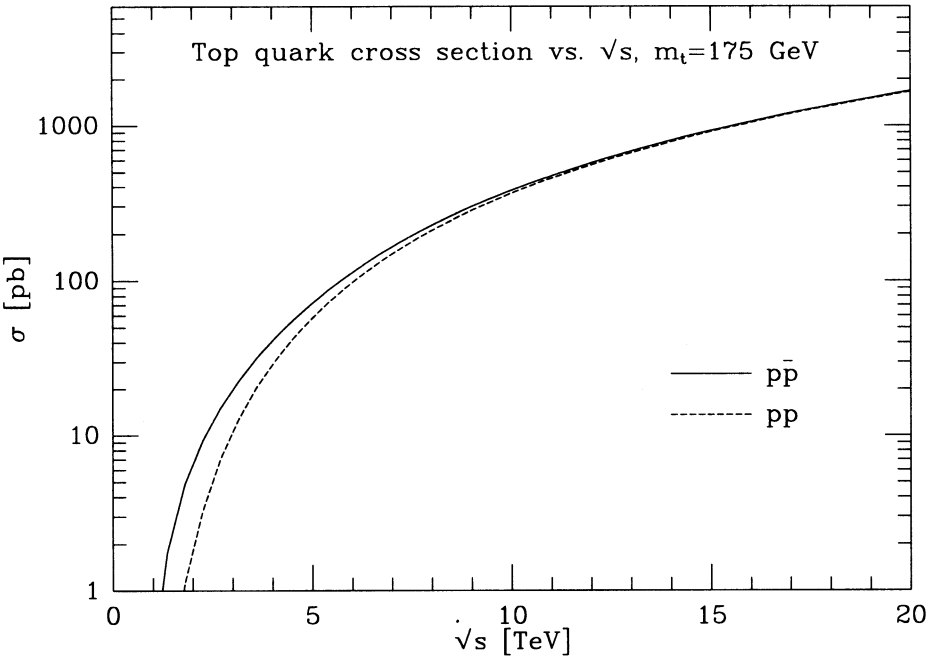


Fig. 10.22. The cross section for top quark production versus energy.

Downloaded from https://www.cambridge.org/core. UNIVERSIDAD AUTONOMA METROPOLITANA, on 17 Nov 2026 at 02:28:30, subject to the Cambridge Core terms of use, available at https://www.cambridge.org/core/terms. https://doi.org/10.1017/CBO9780511628788.011

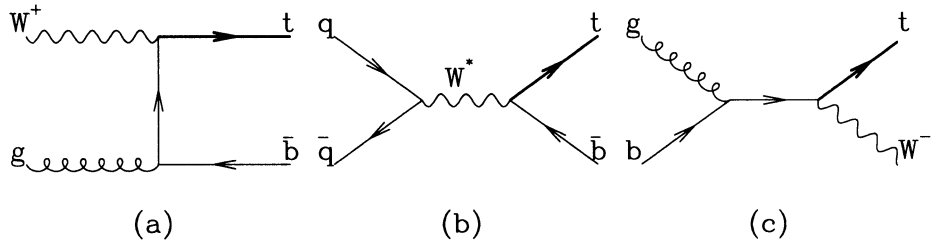


Fig. 10.23. Diagrams for single top production.

Because the top quark is so heavy, we can think of paying the price of a weak interaction in order to have the advantage of producing only a single top [53]. Three possible single-top quark production mechanisms are

$$(a) \quad Wg \to t\bar{b}\,, \tag{10.90}$$

$$(b) \quad q\bar{q} \to t\bar{b}\,, \tag{10.91}$$

$$(c) \quad gb \to tW^-\,. \tag{10.92}$$

Representative diagrams are shown in Fig. 10.23. It is found that the raw rate for these processes as observed in the lepton + jets channel is at least a factor of ten below the standard production mechanism at $\sqrt{s} = 1.8$ TeV, as shown in Fig. 10.24. A measurement of the single top cross section will place a constraint on V_{tb} [9].

10.6 Heavy quarks in jets

10.6.1 Fragmentation functions for heavy quarks

Parton model calculations predict the rates for heavy quark production. It is, however, the decay products of a heavy hadron that are actually observed. The process of fragmentation, *viz.* the attachment of a light antiquark $\bar{q}$ to a heavy quark Q leads to only a slight deceleration of the latter. Following [54] we can model the amplitude for a rapidly moving heavy quark Q of momentum P to fragment into a hadron $H = Q\bar{q}$ of momentum zP and a light quark q (Fig. 10.25) by calculating the energy difference before and after fragmentation,

$$\begin{aligned}\Delta E &= E_Q - E_H - E_q \\ &= \sqrt{m_Q^2 + P^2} - \sqrt{m_H^2 + z^2P^2} - \sqrt{m_q^2 + (1-z)^2P^2} \\ &\approx \frac{m_Q^2}{2P}\Big[1 - \frac{1}{z} - \frac{\epsilon_Q}{1-z}\Big]\end{aligned} \tag{10.93}$$

Downloaded from https://www.cambridge.org/core. UNIVERSIDAD AUTONOMA METROPOLITANA, on 17 Nov 2026 at 02:28:30, subject to the Cambridge Core terms of use, available at https://www.cambridge.org/core/terms. https://doi.org/10.1017/CBO9780511628788.011

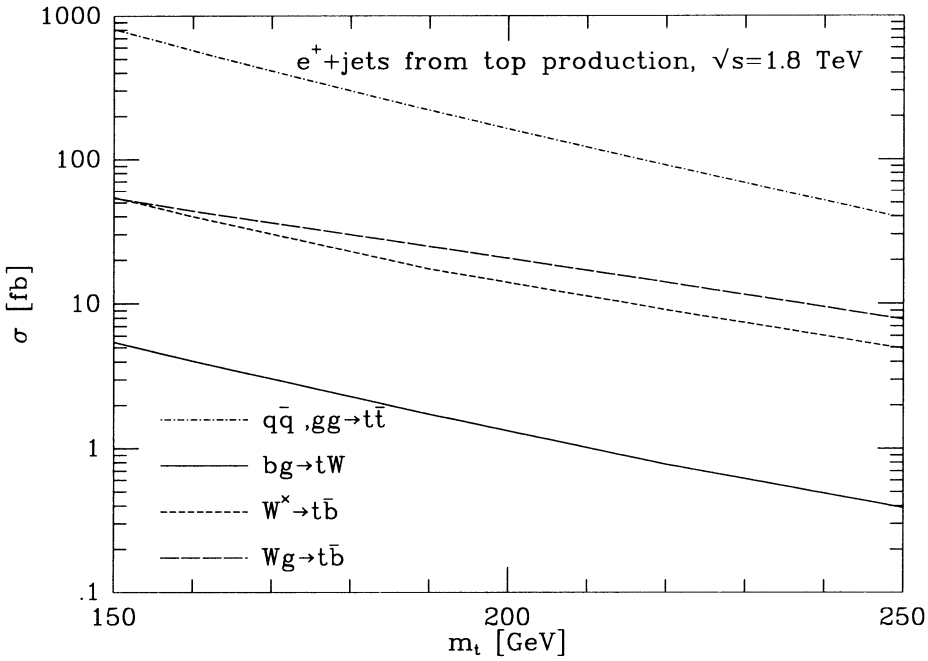


Fig. 10.24. The cross section for positron + jets versus top quark mass.

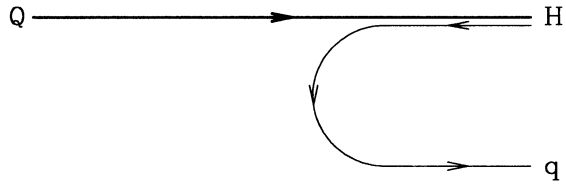


Fig. 10.25. Model for heavy quark fragmentation.

where $\epsilon_Q = m_q^2/m_Q^2$ and we have taken $m_H = m_Q$ for simplicity. The transition amplitude is modelled by the energy denominator, $T \simeq 1/\Delta E$. Squaring the amplitude and including a factor of $1/z$ for longitudinal phase space, we obtain the *Peterson function* for the fragmentation of a heavy quark Q into a heavy hadron H:

$$D_Q^H(z) = \frac{N_H}{z}\left[1 - \frac{1}{z} - \frac{\epsilon_Q}{1-z}\right]^{-2} . \tag{10.94}$$

The normalization factors N_H are constrained by the sum over all hadrons containing the heavy quark:

$$\sum_H \int dz\, D_Q^H(z) = 1 . \tag{10.95}$$

Downloaded from https://www.cambridge.org/core. UNIVERSIDAD AUTONOMA METROPOLITANA, on 17 Nov 2026 at 02:28:30, subject to the Cambridge Core terms of use, available at https://www.cambridge.org/core/terms. https://doi.org/10.1017/CBO9780511628788.011

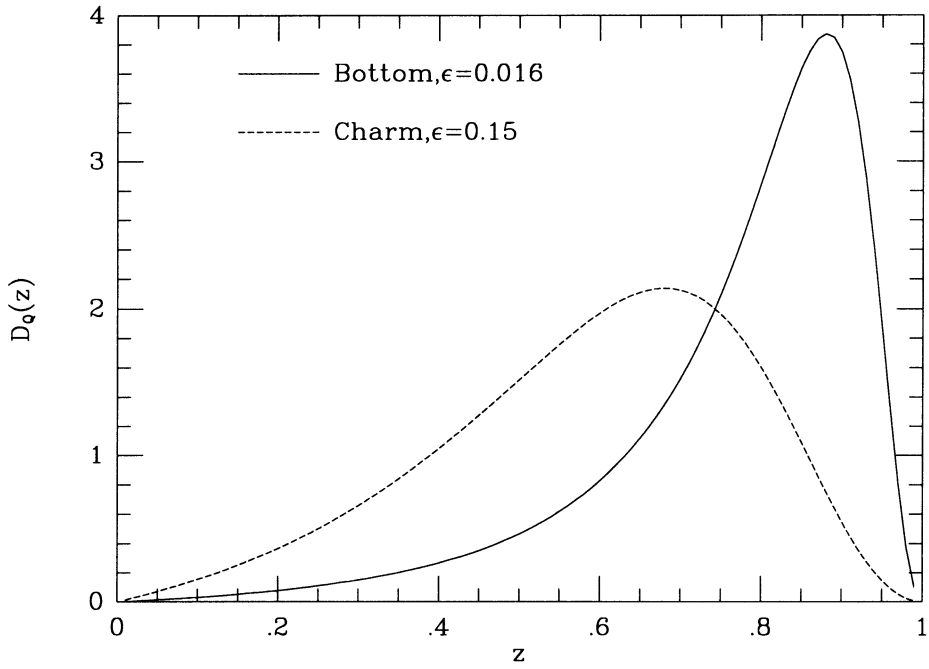


Fig. 10.26. The Peterson model for b and c fragmentation functions.

The Peterson function is plotted in Fig. 10.26 for $\epsilon_c = 0.15$ and $\epsilon_b = 0.016$. In principle, ϵ_Q is fixed by the heavy and light quark masses, but in practice it is treated as a free parameter.

10.6.2 Heavy quarks in gluon jets

Another question of experimental interest is the frequency with which heavy quarks are found amongst the fragmentation products of a light quark or gluon jet. Since hadrons containing heavy quarks have appreciable semi-leptonic branching ratios, such events will often lead to final states with leptons in jets. If we wish to use lepton plus jet events as a signature for new physics we must understand the background due to heavy quark production and decay.

This issue is logically unrelated to the total heavy quark cross section. As discussed above, the total cross section is dominated by events with a small transverse energy, of the order of the quark mass m. Jet events inhabit a different region of phase space, since they contain a cluster of transverse energy $E_T \gg m$. This kinematic region gives a small contribution to the total heavy quark cross section.

A gluon fragmenting into a heavy quark pair must have a virtuality $k^2 >$

Downloaded from https://www.cambridge.org/core. UNIVERSIDAD AUTONOMA METROPOLITANA, on 17 Nov 2026 at 02:28:30, subject to the Cambridge Core terms of use, available at https://www.cambridge.org/core/terms. https://doi.org/10.1017/CBO9780511628788.011

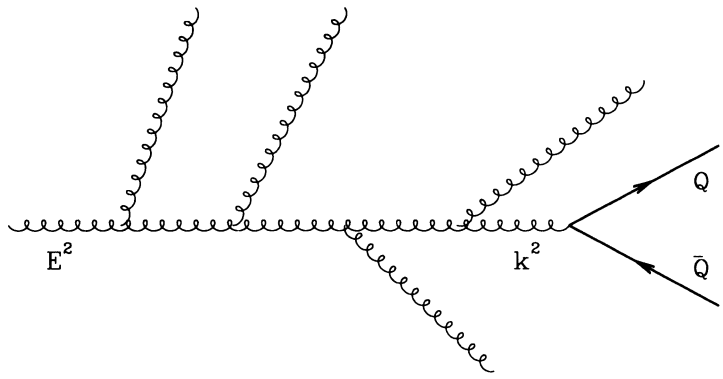


Fig. 10.27. Heavy quark production in jets.

$4m^2$ and so perturbative methods should be applicable for a sufficiently heavy quark. The number of $Q\bar{Q}$ pairs per gluon jet is calculable [55] from diagrams such as the one shown in Fig. 10.27. The calculation has two parts. First one has to calculate $n_g(E^2, k^2)$, the number of gluons of off-shellness k^2 inside a jet produced in a hard process at scale E^2. Secondly, one needs the transition probability for a gluon with off-shellness k^2 to split into a pair of heavy quarks.

The number of gluons of virtual mass-squared k^2 inside a gluon jet produced at scale E^2 is given by [55]

$$n_g(E^2, k^2) \simeq \left[\frac{\ln(E^2/\Lambda^2)}{\ln(k^2/\Lambda^2)}\right]^a \cosh\left\{\sqrt{\frac{2C_A}{\pi b}}\left[\sqrt{\ln\left(\frac{E^2}{\Lambda^2}\right)} - \sqrt{\ln\left(\frac{k^2}{\Lambda^2}\right)}\right]\right\} \tag{10.96}$$

where

$$a = -\frac{1}{4} - \frac{5n_f}{54\pi b} \tag{10.97}$$

(*cf.* Eq. (6.38)), b being the first coefficient in the expansion of the β function, Eq. (10.65). The calculation of the gluon multiplicity (10.96) requires the imposition of the angular ordering constraint which takes into account the coherence of the emitted soft gluons [56], as discussed in Chapter 5. In fact Eq. (10.96) is closely related to the average jet multiplicity (6.110). See refs. [57,58] for more detailed discussion, and for the extension to light quark jets.

Defining $R_{Q\overline{Q}}$ as the mean number of $Q\overline{Q}$ pairs per gluon jet, and ignoring for the moment the gluon branching calculated above, one finds

$$R_{Q\overline{Q}} = \int_{4m^2}^{E^2} \frac{dk^2}{k^2}\frac{\alpha_S(k^2)}{2\pi}\int_{z_-}^{z_+}\frac{1}{2}\left[z^2 + (1-z)^2 + \frac{2m^2}{k^2}\right]dz \tag{10.98}$$

Downloaded from https://www.cambridge.org/core. UNIVERSIDAD AUTONOMA METROPOLITANA, on 17 Nov 2026 at 02:28:30, subject to the Cambridge Core terms of use, available at https://www.cambridge.org/core/terms. https://doi.org/10.1017/CBO9780511628788.011

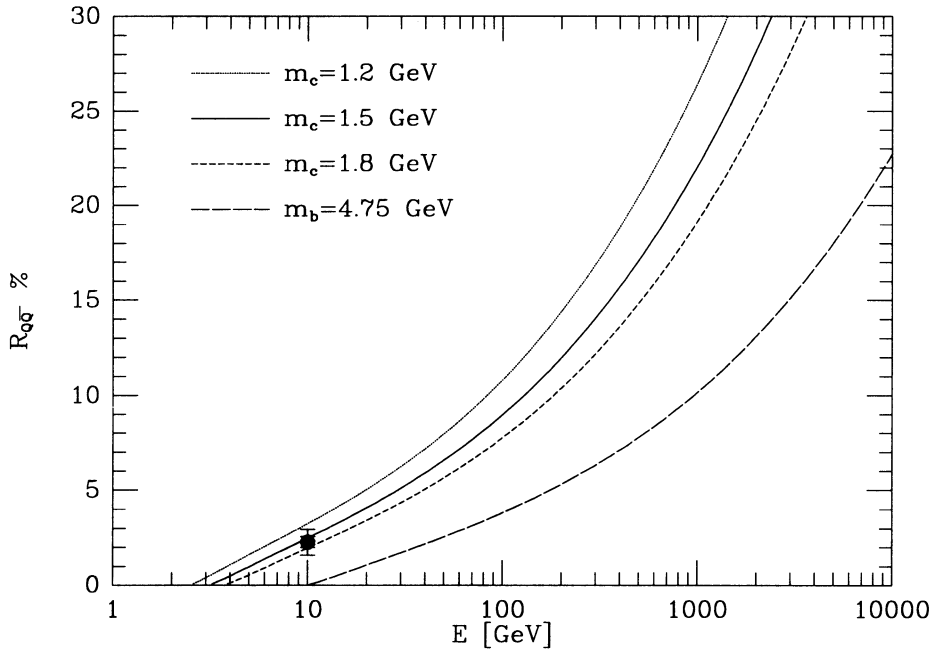


Fig. 10.28. Heavy quarks in gluon jets compared with OPAL data on charm [59].

where the longitudinal momentum fraction of the heavy quark, is denoted by z, for which the integration limits are $z_\pm = (1 \pm \beta)/2$ with $\beta = \sqrt{(1 - 4m^2/k^2)}$. The z-integrand is the Altarelli-Parisi splitting function for $g \to q\bar{q}$, generalized to massive quarks. To take gluon branching into account one should include the multiplicity factor $n_g(E^2, k^2)$. Performing the z integration, one then obtains

$$R_{Q\overline{Q}} = \frac{1}{6\pi} \int_{4m^2}^{E^2} \frac{dk^2}{k^2} \alpha_S(k^2) \left[1 + \frac{2m^2}{k^2}\right] \sqrt{1 - \frac{4m^2}{k^2}}\, n_g(E^2, k^2) \,. \qquad (10.99)$$

The predicted number of charm quark pairs per jet is shown for three values of the charm quark mass in Fig. 10.28, using a value of $\Lambda^{(3)} = 300$ MeV. Also shown is the prediction for the number of bottom quarks per jet, with $\Lambda^{(4)} = 260$ MeV. The OPAL data point [59] was obtained from three-jet events at LEP, by assuming that the lowest-energy jet is a gluon and lepton-tagging charm quarks in that jet.

Downloaded from https://www.cambridge.org/core. UNIVERSIDAD AUTONOMA METROPOLITANA, on 17 Nov 2026 at 02:28:30, subject to the Cambridge Core terms of use, available at https://www.cambridge.org/core/terms. https://doi.org/10.1017/CBO9780511628788.011

10.7 Quarkonium

10.7.1 Quarkonium spectrum

In November 1974 a narrow vector state of mass 3.1 GeV decaying into e^+e^- and $\mu^+\mu^-$ was discovered simultaneously at Brookhaven and SLAC [60]. At the time many explanations were given, but it was soon established that the observed particle was a bound state of a heavy quark-antiquark pair $Q\overline{Q}$. The particle, named the J/ψ, is an s-wave, $J = 1$ bound state of charm quarks, $c\bar{c}$, described in spectroscopic notation $(^{2S+1}L_J)$ as $^3S_1$. The analogous bound state made up of $b\bar{b}$ (and called the Υ) was discovered at Fermilab in 1977 [61]. Many levels of these $Q\overline{Q}$ systems have subsequently been discovered and their spectra will be described below.

In 1974 the surprise was that the J/ψ had a width of only 88 keV, much narrower than one would expect for a hadronically decaying resonance of such a high mass. Early theoretical work [62] provided an explanation, suggesting that heavy quark-antiquark bound states should be narrow because of asymptotic freedom, exploiting the analogy with positronium which is a QED bound state of an electron and a positron.

To understand the correspondence of the quarkonium system with positronium it may be helpful to recall some formulae for the latter system. In these formulae μ denotes the reduced mass, $\mu = m_e/2$. (The same formulae are also true for the hydrogen atom with the appropriate substitution for the reduced mass.) In natural units where $\hbar = c = 1$, the Bohr radius, which sets the scale of atomic sizes, is given by $a_0 = 1/(\alpha\mu)$ where α is the electromagnetic fine structure constant. The scale of the excitation energies of the atom is set by the Rydberg, $\mathcal{R} = \frac{1}{2}\mu\alpha^2$ and energy levels are given by

$$E_n = -\frac{\mathcal{R}}{n^2}\,, \tag{10.100}$$

where n is the principal quantum number. In the non-relativistic limit the energy levels are determined by the principal quantum number alone. Moreover for a spherical symmetric potential of the form $V \sim r^k$ we have from the virial theorem that the expectation values of the kinetic and potential energies are related by

$$2\langle T\rangle = k\langle V\rangle\,, \tag{10.101}$$

where T and V are the kinetic and potential energies respectively. Therefore for a Coulombic system we have that

$$\mu v^2 = 2\langle T\rangle = -2E_1 = \mu\alpha^2 \tag{10.102}$$

and hence that the average velocity v is of order α. Therefore, in as

Downloaded from https://www.cambridge.org/core. UNIVERSIDAD AUTONOMA METROPOLITANA, on 17 Nov 2026 at 02:28:30, subject to the Cambridge Core terms of use, available at https://www.cambridge.org/core/terms. https://doi.org/10.1017/CBO9780511628788.011

much as the coupling is small, the system will be non-relativistic. For a Coulomb potential the wave function is given by the product of an angular factor and a radial wave function. Thus for the lowest-lying s-wave state we have

$$\psi(r,\theta,\phi) = \frac{1}{\sqrt{4\pi}} R_0(r), \quad R_0(r) = 2\left(\frac{1}{a_0}\right)^{\frac{3}{2}} \exp(-r/a_0)\,, \tag{10.103}$$

where the subscript indicates the angular momentum quantum number, L. The square modulus of the radial wave function at the origin for this state is

$$|R_0(0)|^2 = \frac{4}{a_0^3} = 4\alpha^3\mu^3\,. \tag{10.104}$$

For the lowest-lying p-wave state, the derivative of the square modulus of the wave function at the origin is given by

$$|R_1'(0)|^2 = \frac{1}{24a_0^5} = \frac{1}{24}\alpha^5\mu^5. \tag{10.105}$$

The charge conjugation parity of a fermion-antifermion system is given by $C = (-1)^{L+S}$, so that the $^1S_0$ state (parapositronium) has the shortest lifetime since it can decay into two photons. The decay rate is determined by the product of the annihilation probability at rest and the probability of finding the e^+ and e^- at the same point,

$$\Gamma(^1S_0 \to 2\gamma) = \frac{\alpha^2}{m_e^2}|R_0(0)|^2 = \tfrac{1}{2}\alpha^5 m_e\,. \tag{10.106}$$

Because of its odd C-parity the $^3S_1$ state (orthopositronium) can only decay to an odd number of photons. The dominant contribution comes from the decay to three photons for which the decay rate is given by

$$\Gamma(^3S_1 \to 3\gamma) = \frac{\alpha^3}{m_e^2}\frac{4(\pi^2-9)}{9\pi}|R_0(0)|^2 = \frac{2(\pi^2-9)}{9\pi}\alpha^6 m_e\,. \tag{10.107}$$

We shall now proceed to use these facts in our discussion of quarkonium.

The analogy with positronium has given rise to a non-relativistic potential model for quarkonium [62,63]. The model replaces photons by gluons and the electromagnetic fine structure constant by α_S times colour factors. The system will be non-relativistic with the typical velocity v given by α_S evaluated at a scale corresponding to the typical size of the bound state

$$v \sim \alpha_S(1/r^2),\ r \sim \frac{1}{mv}\,. \tag{10.108}$$

Since the velocity v is larger than $\alpha_S(m^2)$, higher-order corrections to the non-relativistic approximation are potentially more important than

Downloaded from https://www.cambridge.org/core. UNIVERSIDAD AUTONOMA METROPOLITANA, on 17 Nov 2026 at 02:28:30, subject to the Cambridge Core terms of use, available at https://www.cambridge.org/core/terms. https://doi.org/10.1017/CBO9780511628788.011

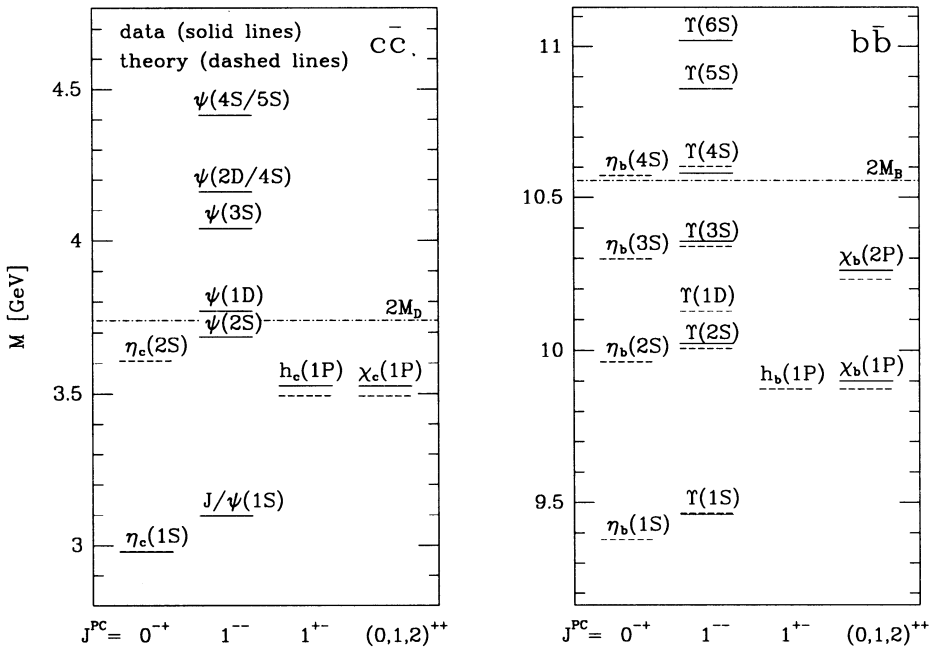


Fig. 10.29. Quarkonium spectra for charmonium and bottomonium.

higher-order perturbative corrections. Detailed results suggest that for the charmonium system $v^2 \approx 0.23c^2$ and for bottomonium $v^2 \approx 0.08c^2$.

The measured states are denoted by solid lines in Fig. 10.29 which shows that the measured energy levels do not depend only on the principal quantum number, n. In particular, the $2S$ and $1P$ levels are split, whereas for a non-relativistic Coulombic system they would be expected to be degenerate, Eq. (10.100). Therefore a more general potential is required. This is not unexpected since the Bohr radius is of order $a_0 \sim 1/(\alpha_S(1/r^2)\mu)$ which is too large to expect simple ideas based on one gluon exchange to apply. The spectra of charmonium and bottomonium are sensitive to the potential at radii between $1/4$ fm $< r <$ 1 fm. The results of a calculation of the interquark potential using lattice QCD have been presented in Section 2.6.

A good description of the spectrum can be obtained using a potential which has an approximately Coulomb form at small distances,

$$V(r) \sim -\frac{4}{3}\frac{\alpha_S(1/r^2)}{r} \tag{10.109}$$

and is confining at large distances

$$V(r) \sim Kr \tag{10.110}$$

Downloaded from https://www.cambridge.org/core. UNIVERSIDAD AUTONOMA METROPOLITANA, on 17 Nov 2026 at 02:28:30, subject to the Cambridge Core terms of use, available at https://www.cambridge.org/core/terms. https://doi.org/10.1017/CBO9780511628788.011

where K is the string tension.

This potential model is successful in describing the spectra of the charmonium and bottomonium states. Fig. 10.29 shows the measured spectra (solid lines) from [3] compared with the predictions [64] of the potential model (dashed lines) using a Buchmüller-Tye potential [65]. This potential satisfies the asymptotic properties specified in Eq. (10.109) and (10.110), but in addition includes the effects of two-loop running at small distances and an interpolation between the limits of small and large r.

10.7.2 Quarkonium decays

Generalizing Eqs. (10.107) to the case of decay to three gluons, we find in the non-relativistic potential model that the width of the $^3S_1$ states, J/ψ and Υ, is

$$\Gamma(^3S_1 \to 3 \text{ gluons}) = \frac{5}{18}\frac{\alpha_S^3}{m^2}\frac{4(\pi^2-9)}{9\pi}|R_0(0)|^2\,, \tag{10.111}$$

where m is the mass of the quark. The extra colour factor with respect to Eq. (10.107) is given by

$$\frac{1}{3}\left[\frac{1}{4}\mathrm{Tr}\{t^A,\{t^B,t^C\}\}\right]^2 = \frac{5}{18}\,, \tag{10.112}$$

where Eq. (1.20) has been used in evaluating the anticommutators. The three gluons subsequently transform into light hadrons with unit probability, so Eq. (10.111) predicts the width of the J/ψ and Υ into light hadrons. The corresponding formula for the $^1S_0$ states, η_c and η_b is

$$\Gamma(^1S_0 \to \text{hadrons}) = \frac{2}{3}\frac{\alpha_S^2}{m^2}|R_0(0)|^2 \tag{10.113}$$

where the colour factor is

$$\frac{1}{3}\left[\frac{1}{2}\mathrm{Tr}\{t^A,t^B\}\right]^2 = \frac{2}{3}. \tag{10.114}$$

Eqs. (10.113) and (10.115) lead to the prediction that the J/ψ should be narrower than the η_c by a factor of

$$\frac{\Gamma(J/\psi \to \text{ light hadrons})}{\Gamma(\eta_c \to \text{ light hadrons})} = \alpha_S\frac{5(\pi^2-9)}{27\pi}. \tag{10.115}$$

The wave function at the origin can be deduced from the leptonic width

$$\Gamma(^3S_1 \to e^+e^-) = \frac{\alpha^2 Q_f^2}{m^2}|R_0(0)|^2. \tag{10.116}$$

The above decay formulae are based on the non-relativistic potential model rather than being derived from QCD. The modern theory of

Downloaded from https://www.cambridge.org/core. UNIVERSIDAD AUTONOMA METROPOLITANA, on 17 Nov 2026 at 02:28:30, subject to the Cambridge Core terms of use, available at https://www.cambridge.org/core/terms. https://doi.org/10.1017/CBO9780511628788.011

quarkonium production and decay [66] is based on a systematic approximation to the full QCD Lagrangian known as Non-Relativistic QCD, (NRQCD). Quarkonia are described in NRQCD in terms of a Fock state decomposition. Thus, for example, the wave function of an S-wave orthoquarkonium vector meson may schematically be written as,

$$|\psi_Q\rangle = O(1)|Q\overline{Q}[^3S_1^{(1)}]\rangle + O(v)|Q\overline{Q}[^3P_J^{(8)}]g\rangle + O(v^2)|Q\overline{Q}[^1S_0^{(8)}]g\rangle + O(v^2)|Q\overline{Q}[^3S_1^{(1,8)}]gg\rangle + O(v^2)|Q\overline{Q}[^3D_J^{(1,8)}]gg\rangle + \cdots . \tag{10.117}$$

The spin, orbital and total angular momentum quantum numbers of the $Q\overline{Q}$ pairs in each Fock component are indicated within the square brackets in spectroscopic notation. In each component of the wave function the $Q\overline{Q}$ pair is either in a singlet or an octet state, denoted by the superscript in brackets. The lowest-order term in the velocity expansion corresponds to the wave function of the non-relativistic potential model and higher order terms correspond to Fock components having additional gluons. The order in the velocity expansion at which each of these Fock states participates in production or decay of the state ψ_Q is governed by simple NRQCD counting rules [66]. The consistent treatment of quarkonium decays requires a formalism which systematically includes all terms at a given order in the velocity v.

A complete treatment of the decays of quarkonium in NRQCD is beyond the scope of this book. We will discuss briefly when the non-relativistic potential model is expected to work and present the results of an analysis of p-wave decays in which it fails. The success of the potential model is based upon two facts. First, the dominant effect of the exchange of gluons is to produce an instantaneous interaction. Since the energy of the exchanged gluons is of order mv^2 and their momentum of order mv, the typical interaction time Δt_I is less than the typical time associated with the interactions of the quarks

$$\Delta t_I \sim 1/(mv) \ll \Delta t_M \sim 1/(mv^2) . \tag{10.118}$$

Second, the probability of finding an extra gluon in the wave function is small, as shown in Eq. (10.117). Since these effects are suppressed by extra powers of the velocity they are relativistic corrections.

For s-wave decays the potential model is equivalent to NRQCD in the approximation in which only the leading terms are retained. In NRQCD, Eqs. (10.113,10.115) and (10.116) are correct if we neglect corrections of relative order v^2. The advantage of NRQCD for s-wave decays is that it provides a systematic method of including the relativistic corrections.

In the potential model the width for the p-wave decays is proportional to the derivative of the wave function at the origin, which is of order m^5v^5, as can be seen from Eq. (10.105). However in NRQCD a leading

Downloaded from https://www.cambridge.org/core. UNIVERSIDAD AUTONOMA METROPOLITANA, on 17 Nov 2026 at 02:28:30, subject to the Cambridge Core terms of use, available at https://www.cambridge.org/core/terms. https://doi.org/10.1017/CBO9780511628788.011

contribution can also be obtained by taking an octet $Q\overline{Q}$ component of the wave function, which also leads to a net contribution of order v^5. For the p-wave states the leading NRQCD results for the decay are [66]

$$\begin{aligned}
\Gamma(^3P_0 \to \text{hadrons}) &= 6\frac{\alpha_S^2}{m^4}|R_1'(0)|^2 + \frac{\alpha_S^2 \pi n_f}{3m^2}\langle\chi_{c0}|\mathcal{O}_8(^3S_1)|\chi_{c0}\rangle\,, \\
\Gamma(^3P_1 \to \text{hadrons}) &= \frac{\alpha_S^2 \pi n_f}{3m^2}\langle\chi_{c1}|\mathcal{O}_8(^3S_1)|\chi_{c1}\rangle\,, \\
\Gamma(^3P_2 \to \text{hadrons}) &= \frac{8}{5}\frac{\alpha_S^2}{m^4}|R_1'(0)|^2 + \frac{\alpha_S^2 \pi n_f}{3m^2}\langle\chi_{c2}|\mathcal{O}_8(^3S_1)|\chi_{c2}\rangle\,, \\
\Gamma(^1P_1 \to \text{hadrons}) &= \frac{\alpha_S^2 \pi (N^2-4)}{2Nm^2}\langle h_c|\mathcal{O}_8(^1S_0)|h_c\rangle\,. \qquad (10.119)
\end{aligned}$$

The above formulae are valid in order v^5 and are subject to corrections of higher order in v and in α_S. The symbol h_c (χ_{cJ}) denotes the wave function of the $^1P_1$ (^3P_J) state and $\mathcal{O}_8(^1S_0)$ is an operator containing four heavy quark fields with both quark-antiquark pairs in a $J = 0$, colour octet state. Because of the necessity of retaining the colour octet component, the non-relativistic potential model fails to describe the complete leading term in P-state decays. Eqs. (10.119) contain four new unknown matrix elements which to leading order are related by heavy quark symmetry,

$$\langle\chi_{cJ}|\mathcal{O}_8(^3S_1)|\chi_{cJ}\rangle = \langle h_c|\mathcal{O}_8(^1S_0)|h_c\rangle\Big(1 + O(v^2)\Big), \quad J = 0, 1, 2\,. \quad (10.120)$$

As a result, at lowest order in v^2, only one non-perturbative matrix element is required, in addition to the derivative of the wave function at the origin which is already required in the non-relativistic potential model.

10.7.3 Quarkonium production

The production of muon pairs in hadronic collisions is of great importance because of the ease of triggering on a produced muon pair. Consequently there are many results on quarkonium production in hadronic reactions. Reviews of the data and the theory are contained in refs. [67,68]. The data come both from fixed-target experiments and from high-energy colliders. The new collider data provide information on the transverse momentum dependence of the cross section over a wide range of p_T.

Quarkonium production is also important because it is proposed as a signal for deconfinement in high-energy hadronic or nuclear collisions. For details and references to earlier literature we refer the reader to ref. [69]. After a high-energy collision, multiple interactions will thermalize the system leading to hot, strongly interacting matter. This matter can either be in a confined hadronic phase, or in a deconfined phase known as the

Downloaded from https://www.cambridge.org/core. UNIVERSIDAD AUTONOMA METROPOLITANA, on 17 Nov 2026 at 02:28:30, subject to the Cambridge Core terms of use, available at https://www.cambridge.org/core/terms. https://doi.org/10.1017/CBO9780511628788.011

quark-gluon plasma. The production of quarkonium is one of the preferred places to look for evidence of the quark-gluon plasma. The idea is that, in the deconfined phase, the interquark potential will be screened, leading to a suppression of J/ψ production. Since the J/ψ has a small spatial dimension of order $1/m$, it emerges unscathed from the hadronic system if it is in the confined phase. Quarkonium production will therefore be sensitive to the partonic state of the medium at the moment of its creation. To calculate in detail how the observed rate of quarkonium production depends on the medium we need to understand the standard QCD production mechanisms.

The simplest diagrams which lead to the production of a $Q\overline{Q}$ pair are the lowest-order diagrams shown in Fig. 10.8. However the quark-antiquark annihilation diagram produces a $Q\overline{Q}$ pair in an octet state. The gluon-gluon fusion mechanism can produce a $Q\overline{Q}$ pair in either a singlet or an octet state. The *colour evaporation model* assumes that the colour quantum numbers are adjusted by emitting a soft gluon at no cost in rate and with no dynamical effects [70]. Differential distributions for the production of a given quarkonium state are assumed to be proportional to the rate of production of heavy quarks in the appropriate mass range

$$\frac{d\sigma_H}{dx_F} = A_H \int_{2m}^{2m_D} dm_{Q\overline{Q}} \, \frac{d\sigma}{dm_{Q\overline{Q}} dx_F} \, . \tag{10.121}$$

A_H is a constant independent of x_F which expresses the fact that only a fraction of the cross section in the appropriate mass range contributes to a given quarkonium state. There is little detailed theoretical justification for the colour evaporation model. Nevertheless, the model has had some success describing the x_F distributions and energy dependences of quarkonium production at fixed-target energies. It also predicts rather similar cross sections for $J/\psi, \psi'$ and χ production at fixed-target energies, in accord with observations [67,71].

A more sophisticated approach is the *colour singlet model* in which the wave function of the $Q\overline{Q}$ state is included and the number of gluons needed to arrive at a colour singlet is taken into account explicitly. At order α_S^2 the only diagram which can contribute is shown in Fig. 10.30(a). This diagram (with on-shell incoming gluons) cannot contribute to the production of a $J = 1$ state. This is a consequence of Yang's theorem [74], which states that a spin-one particle cannot couple to two photons, generalized to the case of gluons. Fig. 10.30(a) is expected to be important at high energy because of the large flux of gluons [72]. The rate is calculated to be (see for example ref. [73])

$$\hat{\sigma}(gg \to {}^{2S+1}L_J) = \frac{\pi^2(2J+1)}{16m} \, \Gamma({}^{2S+1}L_J \to gg) \, \delta(\hat{s} - M^2) \, , \tag{10.122}$$

Downloaded from https://www.cambridge.org/core. UNIVERSIDAD AUTONOMA METROPOLITANA, on 17 Nov 2026 at 02:28:30, subject to the Cambridge Core terms of use, available at https://www.cambridge.org/core/terms. https://doi.org/10.1017/CBO9780511628788.011

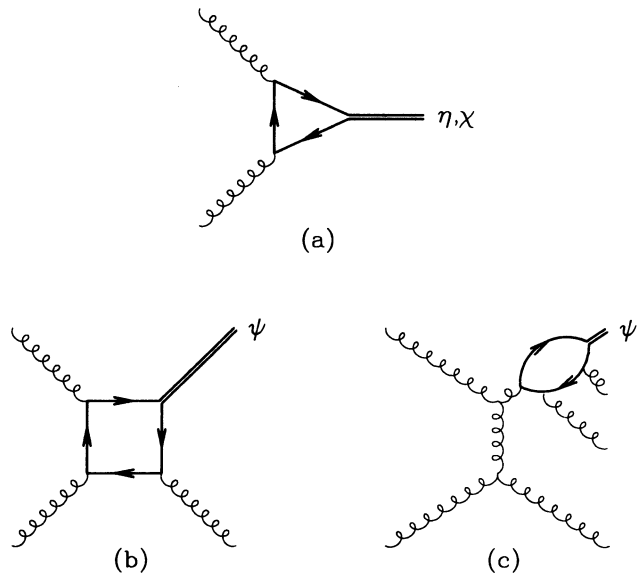


Fig. 10.30. Feynman diagrams in the colour singlet model.

where m is the mass of the quark and $M \approx 2m$ is the mass of the $Q\overline{Q}$ state.

From Eq. (10.113), the result in the non-relativistic potential model for production of the $^1S_0$ state is therefore

$$\hat{\sigma}(gg \to \eta) = \frac{\pi^2 \alpha_S^2}{24m^3} |R_0(0)|^2 \, \delta(\hat{s} - M^2). \tag{10.123}$$

This diagram can also contribute to the production of P states, χ_0 and χ_2. From Eq. (10.119) we find that the partonic cross sections are given in the non-relativistic potential model by [75]

$$\hat{\sigma}(gg \to \chi_0) = \frac{3\pi^2 \alpha_S^2}{8m^5} |R_1'(0)|^2 \, \delta(\hat{s} - M^2), \tag{10.124}$$

$$\hat{\sigma}(gg \to \chi_2) = \frac{\pi^2 \alpha_S^2}{2m^5} |R_1'(0)|^2 \, \delta(\hat{s} - M^2) \, . \tag{10.125}$$

The χ states can decay to a final state containing a J/ψ and hence contribute to the observed signal for J/ψ production. In the colour singlet model the J/ψ and the χ_1 state can only be produced by higher-order diagrams and should therefore be smaller. This prediction is at variance with the data at fixed-target energies, where rather similar rates of J/ψ and χ production are observed [67,76].

In the light of the discussion given above for quarkonium decays, the colour singlet model should be considered to be superseded by NRQCD. The modern QCD description of quarkonium production in hadronic collisions is based on the idea of factorization [66], *i.e.* the separation of the

Downloaded from https://www.cambridge.org/core. UNIVERSIDAD AUTONOMA METROPOLITANA, on 17 Nov 2026 at 02:28:30, subject to the Cambridge Core terms of use, available at https://www.cambridge.org/core/terms. https://doi.org/10.1017/CBO9780511628788.011

short and long distance pieces. Rather than discussing in detail the application of NRQCD to the total cross section we shall turn to the case of quarkonium production at large p_T which is of interest for the description of the most recent collider data [77].

In the colour singlet model at large p_T the diagrams of Fig. 10.30(b) and (c) contribute to J/ψ production [78,79]. Note however that the p_T dependences of the two diagrams is quite different. The diagram in Fig. 10.30(b) is of order α_S^3 but has two hard propagators in the amplitude and hence the cross section falls off like $1/p_T^8$. The diagram in Fig. 10.30(c) on the other hand is of $O(\alpha_S^3)$ but leads to a cross section which falls off as $1/p_T^4$. In the latter diagram only the single exchanged gluon is forced far off mass shell at large p_T.

At large p_T the dominant contribution therefore comes from the diagram which describes the fragmentation of a gluon into a $Q\bar{Q}$ pair. This fragmentation proceeds either via a colour singlet piece requiring the emission of two gluons as shown in Fig. 10.30(c) or via an octet component.

$$D(z,2m) = d_1^{^3S_1}(z,2m)\langle\mathcal{O}(^3S_1^{(1)})\rangle + d_8^{^3S_1}(z,2m)\langle\mathcal{O}(^3S_1^{(8)})\rangle \ . \quad (10.126)$$

The short distance coefficient of the colour octet matrix element can be calculated from the Feynman diagram for $g^* \to Q\overline{Q}$. The result is [80,81],

$$d_8^{^3S_1}(z,2m) = \frac{\alpha_S(4m^2)\pi}{24m^3}\delta(1-z) \ . \quad (10.127)$$

The result for the colour singlet mechanism shown in Fig. 10.30(c) is given in [82,83]. Since it involves a $Q\overline{Q}$ pair and two gluons in the final state it is more complicated than the expression in Eq. (10.127). The singlet matrix element in Eq. (10.126) can be determined by relating it to the wave function at the origin of the potential model

$$\langle 0|\mathcal{O}(^3S_1^{(1)})|0\rangle \approx \frac{3}{2\pi}|R_0(0)|^2 \ , \quad (10.128)$$

where $|R_0(0)|^2$ can be obtained from leptonic width, Eq. (10.116). Since $|R_0(0)|^2$ is of order m^3v^3 the singlet piece leads to a contribution of order $\alpha_S^3 v^3$. The octet piece is of order $\alpha_S v^7$, where the suppression of four powers of v is due to the v^2 suppression of the octet $^3S_1$ piece in Eq. (10.117).

The relative numerical importance of the two mechanisms can be judged by examination of the first moment which can be calculated numerically. The total fragmentation probability is found to be [83]

$$\begin{aligned}\int_0^1 dz\, D(z,2m) &= 8.28\times 10^{-4}\frac{\alpha_S^3(4m^2)}{m^3}\langle\mathcal{O}(^3S_1^{(1)})\rangle \\ &+ 1.31\times 10^{-1}\frac{\alpha_S(4m^2)}{m^3}\langle\mathcal{O}(^3S_1^{(8)})\rangle \ . \quad (10.129)\end{aligned}$$

Downloaded from https://www.cambridge.org/core. UNIVERSIDAD AUTONOMA METROPOLITANA, on 17 Nov 2026 at 02:28:30, subject to the Cambridge Core terms of use, available at https://www.cambridge.org/core/terms. https://doi.org/10.1017/CBO9780511628788.011

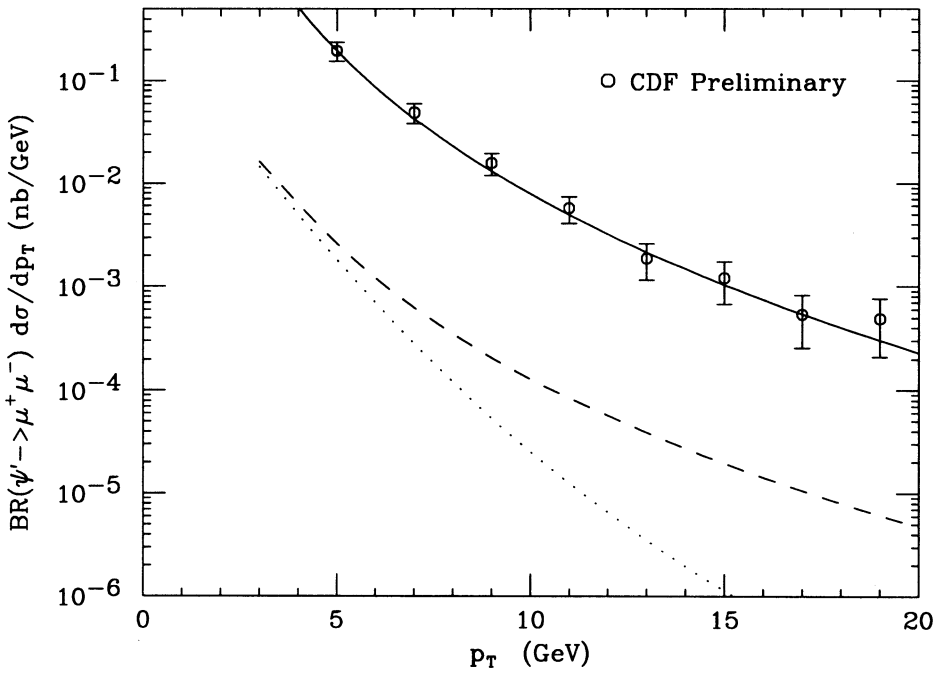


Fig. 10.31. Cross section for ψ' production with colour octet contribution adjusted to the data. Figure from ref. [81].

Fig. 10.31 shows the various contributions to ψ' production. For the ψ' the value of the singlet operator is found using Eq. (10.128) to be,

$$\langle 0|\mathcal{O}(^3S_1^{(1)})|0\rangle \approx 0.11 \text{ GeV}^3 . \tag{10.130}$$

The total leading order contribution (dotted curve) and the total colour singlet fragmentation contribution (dashed curve) both lie below the CDF data, although the fragmentation contribution has the right slope in p_T. Good agreement is found by fitting the colour octet fragmentation term to the data. The value of the matrix element in Eq. (10.126) needed to fit the data is [81]

$$\langle 0|\mathcal{O}(^3S_1^{(8)})|0\rangle = 0.0042 \text{ GeV}^3 \tag{10.131}$$

which is consistent with a suppression of about $O(v^4)$. A full confirmation of this theory of quarkonium production will require comparison with the results from the ψ and Υ systems and direct calculation of the non-perturbative matrix elements.

Downloaded from https://www.cambridge.org/core. UNIVERSIDAD AUTONOMA METROPOLITANA, on 17 Nov 2026 at 02:28:30, subject to the Cambridge Core terms of use, available at https://www.cambridge.org/core/terms. https://doi.org/10.1017/CBO9780511628788.011

References

1) H. Albrecht *et al.*, (ARGUS) *Phys. Lett.* **B255** (1991) 297;
F. Bartelt *et al.*, (CLEO) *Phys. Rev. Lett.* **71** (1993) 4111.

2) B. Grinstein *et al.*, *Phys. Rev.* **D39** (1989) 799.

3) Particle Data Group, L. Montanet *et al.*, *Review of Particle Properties*, *Phys. Rev.* **D50** (1994) 1173.

4) P. Roudeau, Proc. XXVII Int. Conf. on High Energy Physics, Glasgow, July 1994, eds. P.J. Bussey and I.G. Knowles, Institute of Physics Publishing, Bristol (1995), Vol. I, p. 325.

5) Y. Nir, *Phys. Lett.* **B221** (1989) 184.

6) M. Athanas *et al.*, *Phys. Rev. Lett.* **73** (1994) 3503; *ibid.* **74** (1995) 3090(erratum).

7) H. Schröder, *Rep. Prog. Phys.* **52** (1989) 765.

8) I. Bigi *et al.*, *Phys. Lett.* **B323** (1994) 408;
G. Altarelli and S. Petrarca, *Phys. Lett.* **B261** (1991) 303.

9) *Future Electroweak Physics at the Fermilab Tevatron*, Report of the TeV2000 study group, Fermilab-Pub-96/046, eds. D. Amidei and R. Brock.

10) S. Glashow and E. Jenkins, *Phys. Lett.* **B196** (1987) 233.

11) V. Barger and R.J.N. Phillips, *Phys. Rev.* **D41** (1990) 884.

12) S. Glashow and S. Weinberg, *Phys. Rev.* **D15** (1977) 1958.

13) M. Gluck, J.F. Owens and E. Reya, *Phys. Rev.* **D17** (1978) 2324;
B. Combridge, *Nucl. Phys.* **151** (1979) 429.

14) R.K. Ellis, *Strong Interactions and Gauge Theories,* edited by J. Tran Thanh Van, Editions Frontières, Gif-sur-Yvette, 1986, p. 339;
R.K. Ellis, Proceedings of the 17th SLAC summer institute on particle physics, SLAC-REPORT-361, p. 45 (1989).

15) J.C. Collins, D.E. Soper and G. Sterman, *Nucl. Phys.* **B263** (1986) 37

16) S.J. Brodsky, J.C. Collins, S.D. Ellis, J.F. Gunion and A.H. Mueller, in *Proc. 1984 Summer Study on the Design and Utilization of the Superconducting Super Collider*, Fermilab, Batavia, Illinois, 1984, p. 227;
S.J. Brodsky, J.F. Gunion and D.E. Soper, *Phys. Rev.* **D36** (1987) 2710.

17) P. Nason, S. Dawson and R.K. Ellis, *Nucl. Phys.* **B327** (1990) 49; *ibid.* **B335** (1990) 260(erratum).

18) W. Beenakker *et al.*, *Nucl. Phys.* **B369** (1992) 543.

19) P. Nason, S. Dawson and R.K. Ellis, *Nucl. Phys.* **B303** (1988) 607.

20) W. Beenakker, H. Kuijf, W. van Neerven, J. Smith, *Phys. Rev.* **D40** (1989) 54.

21) G. Altarelli *et al.*, *Nucl. Phys.* **B308** (1988) 724.

22) S. Frixione *et al.*, *Nucl. Phys.* **B431** (1994) 453.

23) P. Harriman *et al.*, *Phys. Rev.* **D42** (1990) 798.

24) P.J. Sutton *et al.*, *Phys. Rev.* **D45** (1992) 2349.

25) R.K. Ellis and P. Nason, *Nucl. Phys.* **B312** (1989) 551.

26) E691 collaboration, J.C. Anjos *et al.*, *Phys. Rev. Lett.* **62** (1989) 513; *ibid.* **65** (1990) 2503.

27) NA14 collaboration, M.P. Alvarez *et al.*, *Zeit. Phys.* **C60** (1993) 53.

28) E687 collaboration, G. Bellini, Proceedings of 'Les Rencontres de Physique de la Vallée d'Aoste', La Thuile, 1994.

29) R.K. Ellis, Proc. XXIV Int. Conf. on High Energy Physics, Glasgow, August 1988, eds. R. Kotthaus and J.H. Kühn, Springer-Verlag (1988), p. 48.

30) S.P.K. Tavernier, *Rep. Prog. Phys.* **50** (1987) 1439.

Downloaded from https://www.cambridge.org/core. UNIVERSIDAD AUTONOMA METROPOLITANA, on 17 Nov 2026 at 02:28:30, subject to the Cambridge Core terms of use, available at https://www.cambridge.org/core/terms. https://doi.org/10.1017/CBO9780511628788.011

31) H1 collaboration, S. Aid *et al.*, *Phys. Lett.* **B354** (1995) 494;
ZEUS collaboration, M. Derrick *et al.*, *Phys. Lett.* **B345** (1995) 576.

32) UA1 collaboration, C. Albajar *et al.*, *Zeit. Phys.* **C61** (1994) 41.

33) CDF collaboration, F. Abe *et al.*, *Phys. Rev. Lett.* **68** (1992) 3403; *ibid.* **71** (1993) 500; *ibid.* **71** (1993) 2396; *ibid.* **71** (1993) 2537; *Phys. Rev.* **D50** (1994) 4252.

34) D0 collaboration, S. Abachi *et al.*, *Phys. Rev. Lett.* **74** (1995) 3548.

35) J.C. Collins and R.K. Ellis, *Nucl. Phys.* **B360** (1991) 3.

36) D. Schaile and P.M. Zerwas, *Phys. Rev.* **D45** (1992) 3262;
S.L. Wu, Proceedings of the Lepton Photon Symposium, Hamburg, August 1987;
W. Bartel *et al.*, *Phys. Lett.* **B146** (1984) 437.

37) D. Schaile, Proc. XXVII Int. Conf. on High Energy Physics, Glasgow, July 1994, eds. P.J. Bussey and I.G. Knowles, Institute of Physics Publishing, Bristol (1995), Vol. I, p. 27.

38) LEP electroweak working group, preprint CERN-PPE/95-172.

39) CDF collaboration, F. Abe *et al.*, *Phys. Rev. Lett.* **74** (1995) 2626.

40) D0 collaboration, S. Abachi *et al.*, *Phys. Rev. Lett.* **74** (1995) 2632.

41) A. Caner, Presented at 'Les Rencontres de Physique de la Vallée d'Aoste', March 1996.

42) M. Narain, Presented at 'Les Rencontres de Physique de la Vallée d'Aoste', March 1996.

43) V. Fadin, V. Khoze and T. Sjöstrand, *Zeit. Phys.* **C48** (1990) 613.

44) S. Catani *et al.*, *Phys. Lett.* **B378** (1996) 329.

45) R.K. Ellis, *Phys. Lett.* **B259** (1991) 492.

46) E. Laenen, J. Smith and W. van Neerven, *Phys. Lett.* **B321** (1994) 254.

47) E. Laenen, J. Smith and W. van Neerven, *Nucl. Phys.* **B369** (1992) 543.

48) R.K. Ellis, Proceedings of the 27th International Conference on High Energy Physics, Glasgow, (July 1994).

49) A.D. Martin, R.G. Roberts and W.J. Stirling, *Phys. Lett.* **B356** (1995) 89.

50) D. Bardin *et al.*, preprint CERN–TH 6443/92 (1992).

51) S. Eidelman and F. Jegerlehner, *Zeit. Phys.* **C67** (1995) 585.

52) CDF collaboration, preprint CDF/DOC/PUBLIC/3171;
see also, 'Future Electroweak Physics at the Fermilab Tevatron, Report of the tev 2000 Study Group', Fermilab-Pub-96/082 (1996).

53) S. Dawson, *Nucl. Phys.* **B249** (1985) 42;
S. Willenbrock and D.A. Dicus, *Phys. Rev.* **D34** (1986) 155;
S. Dawson and S. Willenbrock, *Nucl. Phys.* **B284** (1987) 449;
C-P. Yuan, *Phys. Rev.* **D41** (1990) 42;
S. Cortese and R. Petronzio, *Phys. Lett.* **B253** (1991) 494;
R.K. Ellis and S. Parke, *Phys. Rev.* **D46** (1992) 3785;
G. Bordes and B. van Eijk, *Zeit. Phys.* **C57** (1993) 81; *Nucl. Phys.* **B435** (1995) 23.

54) C. Peterson *et al.*, *Phys. Rev.* **D27** (1983) 105.

55) A.H. Mueller and P. Nason, *Phys. Lett.* **B157** (1985) 226.

56) A. Bassetto, M. Ciafaloni and G. Marchesini, *Phys. Rep.* **100** (1983) 201 and references therein.

57) M.L. Mangano and P. Nason, *Phys. Lett.* **B285** (1992) 160.

58) M.H. Seymour, *Zeit. Phys.* **C63** (1994) 99, *Nucl. Phys.* **B436** (1995) 163.

59) OPAL collaboration, R. Akers *et al.*, *Phys. Lett.* **B353** (1995) 595.

60) J.J. Aubert *et al.*, *Phys. Rev. Lett.* **33** (1974) 1404;
J.-E. Augustin *et al.*, *Phys. Rev. Lett.* **33** (1974) 1406.

61) S.W. Herb *et al.*, *Phys. Rev. Lett.* **39** (1977) 252.

62) T. Appelquist and H.D. Politzer, *Phys. Rev. Lett.* **34** (1975) 43.

Downloaded from https://www.cambridge.org/core. UNIVERSIDAD AUTONOMA METROPOLITANA, on 17 Nov 2026 at 02:28:30, subject to the Cambridge Core terms of use, available at https://www.cambridge.org/core/terms. https://doi.org/10.1017/CBO9780511628788.011

63) E.J. Eichten *et al.*, *Phys. Rev. Lett.* **34** (1975) 369.

64) E.J. Eichten and C. Quigg, *Phys. Rev.* **D49** (1994) 5845.

65) W. Buchmüller and S-H.H. Tye, *Phys. Rev.* **D24** (1981) 132.

66) G.T. Bodwin, E. Braaten and G.P. Lepage, *Phys. Rev.* **D51** (1995) 1125.

67) G. Schuler, preprint CERN-TH-7170-94 (1994).

68) E. Braaten, S. Fleming, T.C. Yuan, Ohio State preprint OHSTPY-HEP-T-96-001 (1996), submitted to *Ann. Rev. Nucl. Part. Sci.*.

69) H. Satz, *Nucl. Phys.* **A590** (1995) 63.

70) H. Fritzsch, *Phys. Lett.* **B67** (1977) 217;
M. Glück, J.F. Owens and E. Reya, *Phys. Rev.* **D18** (1977) 162;
J. Babcock, D. Sivers and S. Wolfram, *Phys. Rev.* **D18** (1978) 162.

71) M.L. Mangano, Proceedings of the Xth Topical Workshop on $p\bar{p}$ Collider Physics, preprint CERN-TH/95-190 (1995).

72) S.D. Ellis and M. Einhorn, *Phys. Rev. Lett.* **34** (1975) 1190.

73) R. Gastmans and T.T. Wu, *The ubiquitous photon*, Oxford University Press (1990).

74) C.N. Yang, *Phys. Rev.* **77** (1950) 242.

75) R. Barbieri, R. Gatto and R. Kögerler, *Phys. Lett.* **B60** (1976) 183.

76) R. Gavai *et al.*, *Intl. J. Mod. Phys.* **A10** (1995) 3043.

77) CDF collaboration, F. Abe *et al.*, *Phys. Rev. Lett.* **69** (1992) 3704;
K. Byrum, Proc. XXVII Int. Conf. on High Energy Physics, Glasgow, July 1994, eds. P.J. Bussey and I.G. Knowles, Institute of Physics Publishing, Bristol (1995), Vol. II, p. 989; Fermilab-Conf-94/136.

78) E.L. Berger and D. Jones, *Phys. Rev.* **D23** (1981) 1521;
R. Baier and R. Rückl, *Zeit. Phys.* **C19** (1983) 251.

79) E. Braaten *et al.*, *Phys. Lett.* **B333** (1994) 548;
D.P. Roy and K. Sridhar, *Phys. Lett.* **B339** (1994) 141;
M. Cacciari and M. Greco, *Phys. Rev. Lett.* **73** (1994) 1586.

80) E. Braaten and T.C Yuan, *Phys. Rev.* **D50** (1994) 3176.

81) E. Braaten and S. Fleming, *Phys. Rev. Lett.* **74** (1995) 3327.

82) E. Braaten and T.C Yuan, *Phys. Rev. Lett.* **71** (1993) 1673.

83) E. Braaten and T.C Yuan, *Phys. Rev.* **D52** (1995) 6627.

Downloaded from https://www.cambridge.org/core. UNIVERSIDAD AUTONOMA METROPOLITANA, on 17 Nov 2026 at 02:28:30, subject to the Cambridge Core terms of use, available at https://www.cambridge.org/core/terms. https://doi.org/10.1017/CBO9780511628788.011